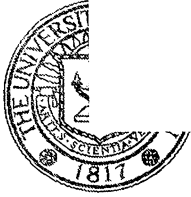


SCI  
MAS

-----  
Thesis



Author

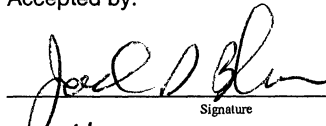
Andrew W. Lammers

Title

4000 Years of Mercury Deposition as  
Recorded in Alaskan Arctic Tundra Soils

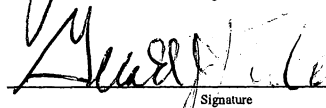
submitted in partial fulfillment  
of the requirements for the degree of  
Master of Science in Geology  
Department of Geological Sciences  
The University of Michigan

Accepted by:

  
Signature

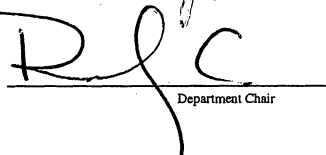
Joel D. Blum  
Name

8/14/06  
Date

  
Signature

Gerald J. Keeler  
Name

8/14/06  
Date

  
Department Chair

RODNEY C. EWING  
Name

8/11/06  
Date

I hereby grant the University of Michigan, its heirs and assigns, the non-exclusive right to reproduce and distribute single copies of my thesis, in whole or in part, in any format. I represent and warrant to the University of Michigan that the thesis is an original work, does not infringe or violate any rights of others, and that I make these grants as the sole owner of the rights to my thesis. I understand that I will not receive royalties for any reproduction of this thesis.

Permission granted.

Permission granted to copy after: \_\_\_\_\_  
Date

Permission declined.

  
Author Signature



# 4000 Years of Mercury Deposition as Recorded in Alaskan Arctic Tundra Soils

A thesis submitted in partial fulfillment of the requirements for the degree of  
Master of Science in Geology

By:

Andrew William Lammers

Department of Geological Sciences  
The University of Michigan  
Ann Arbor, MI

August 2006

## Abstract

Atmospheric mercury depletion events (MDE) occur during springtime in coastal Arctic Alaska and result in elevated concentrations of mercury in the snowpack. It has been suggested that mercury in snow increases in close proximity to open sea ice leads and young sea ice, places where the development of unique snow crystals and the supply of reactive halogens may facilitate mercury deposition. The proportion of mercury deposited during MDE that is re-emitted to the atmosphere from the snow pack versus that deposited onto the tundra during snowmelt is not well known and is under investigation. In the study reported here long-term trends in mercury deposition are investigated with respect to tundra soils in close proximity (<10 km) to coastal areas that frequently see open sea-ice leads and thus young sea ice. Drained thaw lake basins (DTLB) cover about 50% of the land area near Barrow, Alaska and are depositional environments that preserve organic material. As such these basins are a potential archive of atmospherically deposited mercury. Organic matter accumulation begins in DTLB following lake drainage resulting in peat profiles with widely ranging ages dependent on the timing of drainage. Soils were sampled in August of 2005 from 'young' (50-0 yr), 'old' (2000-300 yr), and 'ancient' (5500-2000 yr) DTLB and analyzed for mercury concentration in order to estimate the flux of mercury to the Alaskan Arctic tundra. The modern mercury flux to Barrow, Alaska area tundra soils is  $10.3 \mu\text{g Hg m}^{-2}\text{yr}^{-1}$  compared to a background mercury flux ranging from  $0.61$  to  $1.81 \mu\text{g Hg m}^{-2}\text{yr}^{-1}$ . This range of preindustrial values is consistent with preindustrial mercury fluxes reported for other Arctic locations and for cold regions across the northern hemisphere. The modern flux of mercury in the Barrow area shows a 6 to 17 fold increase over the 'natural' background mercury flux. Additionally, soil core samples were taken from inland sites to assess the difference in the mercury deposition records of coastal and non-coastal Alaskan Arctic areas. Tundra soil samples taken approximately 100 km from Barrow near Atqasuk, Alaska indicate the MDE may be regional in extent rather than a purely coastal phenomenon. Soil samples taken near Fairbanks, AK, approximately 800 km from Barrow, show dissimilar mercury concentration profiles with depth when compared to Arctic soil cores.

## **Table of Contents**

<b>Abstract</b>	<b>ii</b>
<b>Lists of Figures and Tables</b>	<b>iv</b>
<b>Acknowledgements</b>	<b>v</b>
<b>Introduction</b>	<b>1</b>
<b>Study Site</b>	<b>5</b>
Landscape, Climate, Vegetation, Geology	5
Drained Thaw Lake Basins	6
<b>Methods</b>	<b>10</b>
<b>Results</b>	<b>13</b>
Organic Layer Thickness	13
pH	13
Moisture Content	13
Ash Content	14
Bulk Density	17
Mercury Concentration	20
Total Mercury Content	24
<b>Discussion</b>	<b>28</b>
Physical Characteristics of Tundra Soils in Comparison to Peat Bogs	28
The Specter of Cryoturbation	30
Mercury Concentration	31
Total Mercury Content	33
Total Accumulated Mercury	34
Mercury Flux	37
The Merits of Our Method	43
Mercury Depletion Events	43
<b>Conclusions</b>	<b>44</b>
<b>Appendices</b>	<b>46</b>
Appendix A: Field Description of Soil Cores with Depth (cm)	46
Appendix B: Analysis of Solids Samples Using the Nippon Instruments MA-2000 Mercury Analyzer	48
Appendix C: A general statement of AMS protocols and procedures (provided by NOSAMS)	51
Appendix D. Moisture Content Charts	53
Appendix E: Summary of Liquid Analysis Tests With Regards to High Organic Content Samples	55
<b>References</b>	<b>60</b>

## List of Figures

Figure 1. The mercury cycle	2
Figure 2. Mercury deposition as recorded in a Wyoming ice core	3
Figure 3. Map of Alaska	5
Figure 4. Study site map	5
Figure 5. Barrow temperature data for 2005	6
Figure 6. Drained thaw lake basins	8
Figure 7a. Barrow and Atqasuk area ash content	15
Figure 7b. Fairbanks area ash contents	17
Figure 8a. Barrow and Atqasuk area bulk densities	18
Figure 8b. Fairbanks area bulk densities	19
Figure 9. Mercury analysis with and without the purge step	21
Figure 10a. Barrow and Atqasuk area mercury concentrations	25
Figure 10b. Fairbanks area mercury concentrations	24
Figure 10c. Extended mercury profile for core B3	24
Figure 11a. Barrow and Atqasuk area total mercury	25
Figure 11b. Fairbanks area total mercury	26
Figure 12. Mercury accumulation in Alaskan soil cores	35
Figure 13. Mercury accumulation versus core age	36
Figure 14a. Barrow area accumulated mercury versus core age (ages > 590 years)	37
Figure 14b. Barrow area accumulated mercury versus core age (ages < 100 years)	37
Figure 15. Adjusted mercury fluxes	40
Figure 16. Soil core moisture contents	53

## List of Tables

Table 1. Core names, ages, locations, and organic layer thickness	13
Table 2. Moisture content measurement error	14
Table 3. Bulk density measurement error	20
Table 4. Maximum and minimum soil core mercury concentrations	21
Table 5. Mercury analyses precision	22
Table 6. Total mercury content measurement error	25
Table 7. Wet vs. dry site total mercury	27
Table 8. Organic layer mercury accumulation	34
Table 9. Mercury flux calculation results	38
Table 10. Mercury fluxes reported in the literature	41
Table E1. High organic liquids mercury concentration data	55
Table E2. High organic liquids mercury concentration data	56
Table E3. High organic liquids mercury concentration data	57
Table E4. High organic liquids mercury concentration data	57
Table E5. High organic liquids mercury concentration data	58
Table E6. High organic liquids mercury concentration data	59

## **Acknowledgements**

I would like to express my gratitude to those whose guidance, assistance, and support made this work possible. Special thanks go to my advisor Joel Blum who gave me the opportunity to be a part of his research group and to pursue my interests in environmental science and who was instrumental in helping to shape this work at every stage. Thank you also to Jerry Keeler for reading this thesis. Sincere thanks to Abir Biswas for his camaraderie and for the extraordinary amount of time and effort he spent helping me through this process. Thanks to University of Michigan undergraduate students Sara Worsham, Sarah Long, Matt Conrad, Emily Rice and Mike Ritorto for their unflagging help in the lab. Thanks to Ali Kamal, Thomas Douglas, Kenneth Hinkel, Torre Jorgensen, Jerry Brown, and Prethap Kodial for their aid and guidance with the Alaska field work effort. Thanks to Marcus Johnson and Bridget Bergquist for their advice and assistance in the lab. Thanks to Rod Ewing and Udo Becker for their initial guidance and support during my first semester at Michigan. Thank you to my long-time compatriots Brian Collier, Brian Payne, and Eric Vallo for your friendship and inspiration. Thank you to my family especially to Mom, Dad, Carolyn, Charlie, Meg, Phil and Steve for their love, understanding and support. Thank you to my beloved children Adelaide, Jackson, and Norah for your unconditional love and for continuing to remind me of the wonders of life. Finally and foremost, thank you to my wife Mollie for walking with me on this adventure and always.

This work was funded in part by the 2005 and 2006 Scott Turner Awards in Earth Science and by a grant from the National Science Foundation's Office of Polar Programs.

## **Introduction**

Evidence of elevated mercury levels in indigenous Arctic peoples and biota has generated concern among health professionals and wildlife ecologists (AMAP, 2002). Mercury, especially in its organic methylmercury form, is a lipophilic bioaccumulating toxic metal that has been epidemiologically linked to deleterious neurodevelopmental effects such as language, attention, and memory deficits. Most notably, these deficits have been well documented in the Faroe Islands, located between Iceland and Norway in the Arctic (Weihe et al., 1996; Grandjean et al., 1997). Additionally, mercury may inhibit the cardiovascular benefits of a diet rich in healthy fatty acids leading to increases in heart disease among Arctic natives (Rissanen, 2000). Peoples of the Arctic whose subsistence lifestyle incorporates a diet rich in marine mammals and fish, which are known to be high in methylmercury, are likely at risk. The diet of Faroe Island peoples includes a substantial intake of pilot whale meat and blubber that contains elevated levels of methylmercury causing a large portion of the population to exceed the World Health Organization's tolerable weekly intake level of 1.6  $\mu\text{g}/\text{kg}$  body weight (Booth and Zeller, 2005). Mercury poses the greatest danger to the youngest members of such societies, including nursing infants, where impaired memory and motor function have been noted after exposure to presumed safe levels of the contaminant (Zahir et al., 2005).

Of note however, is that epidemiological studies of mercury are few in number, are difficult to carry out, and have produced uncertain results. The presence of confounding factors such as the health impacts of polychlorinated biphenyls (PCBs) that are also found in marine mammal tissues make it difficult to isolate the effects of mercury exposure. One study in the Seychelle Islands (a non-Arctic location) showed no negative impacts of regular low-level dietary mercury exposure on childhood development (Myers et al., 2003). However, the local diet in the Seychelles does not include the consumption of marine mammals as is prevalent in the Arctic.

Mercury is released into the environment via both natural and anthropogenic processes. Natural emissions of mercury include those from volcanoes, degassing of mercury rich rock and soils, and forest fires (Nriagu, 1989). Releases by humans are from coal combustion, waste incineration, metal smelting, cement production, and chlor-alkali industrial processes (Lindquist et al., 1991). Additionally, mercury releases from mining activities have made a significant contribution to total anthropogenic emissions through time (Hylander and Meili, 2003). Mercury emitted by humans is thought to comprise two thirds of the current mercury flux to the environment (Mason et al., 1994).



Mercury primarily moves through the environment in the atmosphere. Atmospheric transport processes have resulted in the global distribution of mercury, bringing contamination to the farthest reaches of the planet (Fitzgerald et al., 1998). Mercury deposition is largely dependent upon the speciation of emitted mercury and upon distance from the emission source. Mercury is emitted as gaseous elemental mercury (GEM) in the form of  $\text{Hg}^0$ , as reactive gaseous mercury (RGM) in the oxidized  $\text{Hg}^{2+}$  form, and as mercury associated with particulate matter. Emitted GEM almost entirely enters the global pool of mercury, avoiding local deposition due to its insoluble/unreactive chemical nature. GEM is gradually oxidized by photochemical reactions in the atmosphere to RGM. RGM is quickly removed from the atmosphere through wet and dry depositional processes.  $\text{Hg}^0$  has an atmospheric residence time of six months to one year, allowing for global transport and distribution (Lamborg et al., 2002). Comprised of soluble/reactive  $\text{Hg}^{2+}$  species, RGM is removed from the atmosphere on a local to regional scale within 100 km of its source (Dvonch et al., 1999). RGM has a short atmospheric residence time and is deposited on the order of several hours (Poissant et al., 2004). Particulate mercury is transported a distance inversely proportional to the aerodynamic diameter (AED) of the particle to which the mercury is sorbed (Godish, 2004). RGM and particulate mercury are largely responsible for local and regional mercury pollution while GEM supplies mercury to the global mercury pool.

Complicating mercury transport and fate are the complex biogeochemical processes that convert mercury among its inorganic and organic species. Upon deposition, microbes can convert inorganic  $\text{Hg}^{2+}$  to methylmercury (MeHg) and demethylate MeHg to  $\text{Hg}^{2+}$ . Also, deposited  $\text{Hg}^{2+}$  can be biologically or photo-chemically reduced to  $\text{Hg}^0$  and re-volatilized to the atmosphere (Morel et al., 1998).

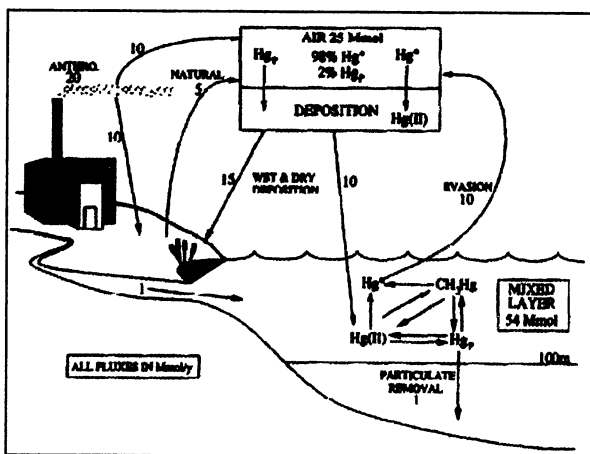


Figure 1. The Mercury Cycle (Mason et al., 1994).

Across the northern hemisphere from Minnesota, U.S.A. to Ontario, Canada and from Greenland to Switzerland, mercury deposition has dramatically increased over background rates since pre-industrial times (Benoit et al., 1998; Givelet et al., 2003; Bindler, 2003; Roos-Barracough et al., 2002a). In addition, pristine locales such as the Wind River Mountains of Wyoming, USA indicate up to a 20-fold increase in mercury deposition over background rates (Schuster et al., 2002). In the Arctic, Alaskan lake sediments, beluga whale teeth, and peat deposits indicate a many-fold increase in mercury deposition rate over the past several centuries (Fitzgerald et al., 2005; Outridge et al., 2002; Shotyk et al., 2005).

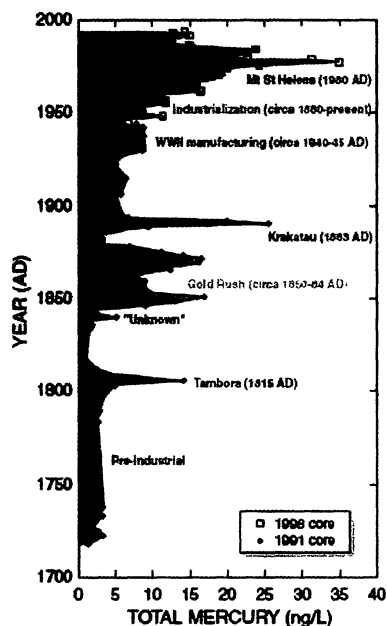
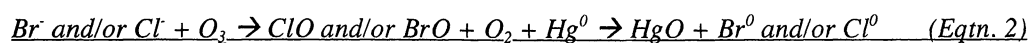
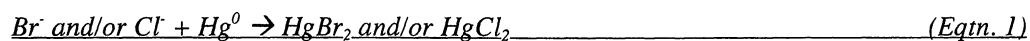


Figure 2. Mercury deposition as recorded in a Wyoming ice core (Schuster et al., 2002).

Observations first made at Alert, Canada (Schroeder et al., 1998) and further described by Lu et al. (2001) point to a newly recognized cause for increased loading of mercury to the Arctic (Lindberg et al., 2002; Skov, 2004). Complex atmospheric processes are causing so-called mercury depletion events (MDE) and may effectively have caused the Arctic to become a mercury sink with respect to the global mercury cycle (Ariya et al., 2004). In the springtime (March-May) after polar sunrise rapid oxidation of tropospheric GEM to RGM and/or particulate mercury in the presence of halogens, coincident with nearly total depletion of tropospheric ozone leads to greatly enhanced mercury deposition. The important reactions to play a part in mercury oxidation are (Lindberg et al., 2002):



Factors promoting the occurrence of MDE seem to include a maritime location, cold (sub -4° C) temperatures, high levels of UV radiation, the presence of reactive halogen radicals, and frozen snow/ice particles. MDE are thought to be a coastal phenomenon because ocean waters likely supply the necessary halogens. After their discovery in the Arctic, MDE were also observed in Antarctica (Ebinghaus et al., 2002).

It has been suggested that mercury depletion events along the northern Alaskan coastline near Barrow, Alaska result in a depositional flux of mercury from January to May of approximately  $55 \mu\text{g m}^{-2}$  (Lindberg et al., 2002) while the annual flux for the northeastern United States, a region containing many known mercury point sources, has been reported at between  $10 \mu\text{g m}^{-2}$  to  $30 \mu\text{g m}^{-2}$  (Bullock, 2000) and 6 to  $14 \mu\text{g m}^{-2}$  (2004 National Atmospheric Deposition Program Mercury Deposition Network Mercury Deposition Summary Report). Snow and frost flower samples from sea ice near Barrow collected during MDE show concentrations up to 820 ng Hg/L (Douglas et al., 2005) while precipitation in the form of rain and snow in the northeastern U.S. averages between 4-10 ng Hg/L (2004 National Atmospheric Deposition Program Mercury Deposition Network Mercury Deposition Summary Report). The springtime pulse of mercury deposited along the northern Alaskan coastline combined with the timing of the deposition, just as ecosystems are becoming increasingly active after winter dormancy, may be creating a harmful scenario for Arctic biota and human populations dependent upon a subsistence lifestyle.

A series of important questions are raised by evidence of enhanced springtime mercury deposition in Arctic Alaska including: What portion of the deposited mercury is revolitized to the atmosphere and what is the resulting net deposition of mercury to the area? What are the post-depositional pathways for mercury through this Arctic ecosystem, specifically where and to what extent is mercury methylated? What are the resultant pools of mercury across the ecosystem?

The work presented here is a study of mercury in the tundra soils near Barrow, Alaska and is primarily concerned with quantifying historical mercury deposition in the area. The following are a list of driving questions: How does the mercury concentration in Alaskan Arctic soil cores change with time? Do soil cores corroborate reports of increasing mercury deposition across the Arctic? What insight does the mercury record give to the spatial extent and occurrence of MDE? What proportion of atmospherically deposited mercury accumulates in peat and is thus retained on the tundra landscape after snowmelt, i.e. what part do tundra soils play in the local mercury cycle?

## Study Site

### *Landscape, Climate, Vegetation, Geology*

The lowland tundra landscape near Barrow, Alaska (figures 3 and 4) is a part of the Arctic Coastal Plain. The region is characterized by numerous ovate lakes, drained lake basins, and small ponds. The surface is marked by extensive networks of low-centered and high-centered frost wedge polygons and has an average relief of 2 to 5 m (Brown et al., 1980). Beneath the surface lies continuous permafrost to a depth of approximately 600 m.

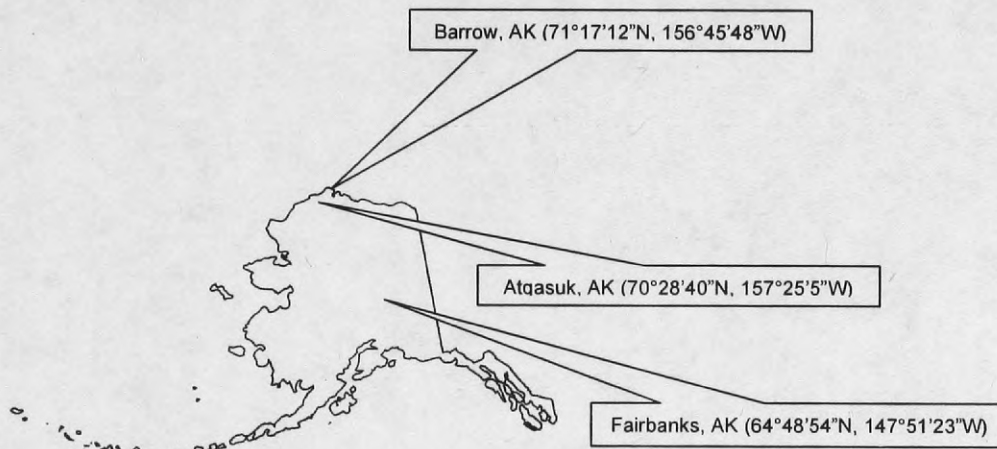


Figure 3. Map of Alaska (from The Alaska Native Knowledge Network)

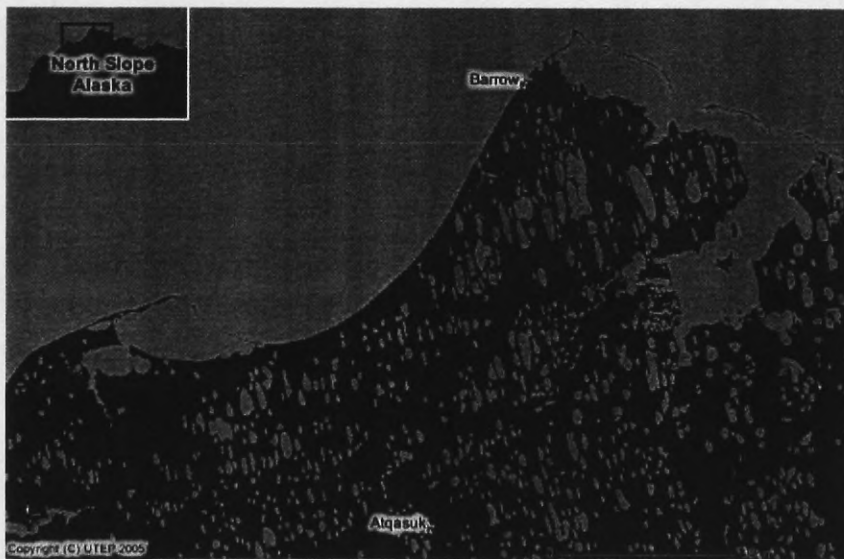


Figure 4. Barrow, Atkasuk and the North Slope of Alaska (Barrow Area Information Database- Internet Map Server)

The average annual maximum temperature in Barrow is  $-9.2^{\circ}\text{C}$  while the average minimum temperature is  $-15.2^{\circ}\text{C}$  (National Climate Data Center). Mean wind speed is 12.5 mph at seven degrees east of north. The Barrow area receives an average of 106 mm of precipitation yearly with 66 mm (63%) falling between July and September. The average annual snowfall is 736 mm and is distributed fairly uniformly from early fall through late spring with October (188 mm) being the month of maximum accumulation. Figure 5 shows daily temperature data for 2005. Fieldwork was conducted in the Barrow area from August 10, 2005 through August 21, 2005. Of note is that the maximum daily temperature for 2005 occurred during this period on August 14<sup>th</sup>.

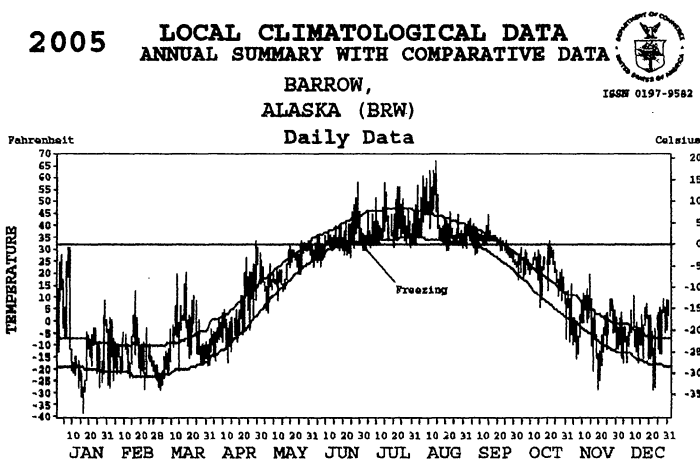


Figure 5. Barrow, Alaska temperature data for 2005 (National Climate Data Center).

Vegetation is typical of Arctic lowland meadow tundra and has limited diversity. Flora composition is dominated by sedges (*Carex aquatilis*) and grasses (*Poa arctica*) with a marked presence of lichens and mosses (*Sphagnum sp.*). Notable is the absence of upright shrubs; woody vegetation is limited to the sparsely occurring least willow (*Salix rotundifolia*). (Brown et al., 1980).

Between approximately 35,000 and 25,000 years before present an inland sea invaded the area (Brown et al., 1980). As sea level regressed, gravelly beach ridge-shoal complexes and entrapped waters remained and the newly exposed surface sediments began to refreeze. At approximately 14,000 years before present the landscape shaping processes that are currently active, principally ice-wedge formation, were in place.

#### Drained Thaw Lake Basins

Ovate lakes cover much of the Arctic Coastal Plain landscape (figure 4). The basins that form when these lakes empty are known as drained thaw lake basins (DTLB). Together the basins and the lakes cover 50-

75% of the landscape (Hussey and Micahelson, 1966). Near Barrow, approximately 50% of the landscape is covered by DTLB (Hinkel et al., 2003). DTLB are of importance to this study because they are depositional environments where organic material is preserved. Organic matter accumulation begins in DTLB following lake drainage when the grasses, sedges and mosses that grow on the newly available surface die and are deposited to the tundra. The cold climate of Arctic Alaska allows for accumulation of organic matter within tundra soils. The organic-rich soils in the uppermost horizon result from the existing imbalance between organic matter deposition and decay that leads to increased soil biomass (FitzPatrick, 1997).

The thaw lake cycle has been thoroughly described (Hopkins, 1949; Britton, 1966; Billings and Peterson, 1980; Mackay, 1988; Hinkel et al., 2003). The cycle is thought to begin when ice-wedges start to grow (at a rate of 0.5 to 1 mm per year) beneath cracks in the surface. Massive ice accumulation causes heaving at the surface around the lateral extent of the growing ice wedges and the beginnings of frost polygons. Relatively low areas develop above ice wedges and ponds form in these depressions. Warm pond waters cause additional melting of the ice wedges below the surface in the center of the forming polygons. As the wedges melt they lose volume and the depressions sink even lower. Eventually small ponds merge to form lakes. Thermal erosion along the lake edges combined with thaw subsidence beneath the lake waters expand the lateral and vertical dimensions of the thaw lakes. Wind generated wave action causes circulation cells to form in the lakes increasing thermal erosion perpendicular to the prevailing summer wind direction. The lakes become oval in shape. In time the thaw lakes drain, sometimes rapidly, due to processes including ice-wedge erosion, headward stream erosion, or coastal erosion. Vegetation is re-established on the site of the drained lake and organic material begins to accumulate above the lake sediments. Eventually new ice wedges develop and the process begins anew.

The tundra soils in the area are acidic, wet and can be grouped into two primary types: inceptisols, mineral soils containing poorly defined horizons, and histosols composed largely of organic material (Brown et al., 1980). The histosols tend to show a three-part morphology with depth. An organic-rich horizon lies directly beneath the surface and is underlain by a bluish clay to silt loam horizon containing intermixed organic material. Below the permafrost table and beneath the clay-silt layer is usually found another organic-rich horizon. The soil stratigraphy is interpreted to indicate the burial of ancient (~12 ka) organic material by lacustrine sediments deposited in thaw lakes followed by the more recent deposition of organic matter after lake drainage.

Hinkel et al. (2003) describe a field-based classification scheme for DTLB supported by C-14 dating in which basins are broken into four age classes: 'young' (less than 50 years old), 'medium' (50-300 years old), 'old' (300-2000 years old), and 'ancient' (2000-5500 years old). As the basins evolve from young to ancient ages the organic layer atop the lacustrine sediments increases in depth, the decomposition of organic material (humification) becomes more complete, frost polygons become further developed, and small ponds in low center polygons increase in extent. The predictable changes in landscape that occur due to ice-wedge evolution and vegetation succession have proven to be useful in sorting basins into age categories even in the absence of radiocarbon derived ages. See basin examples in figure 6.

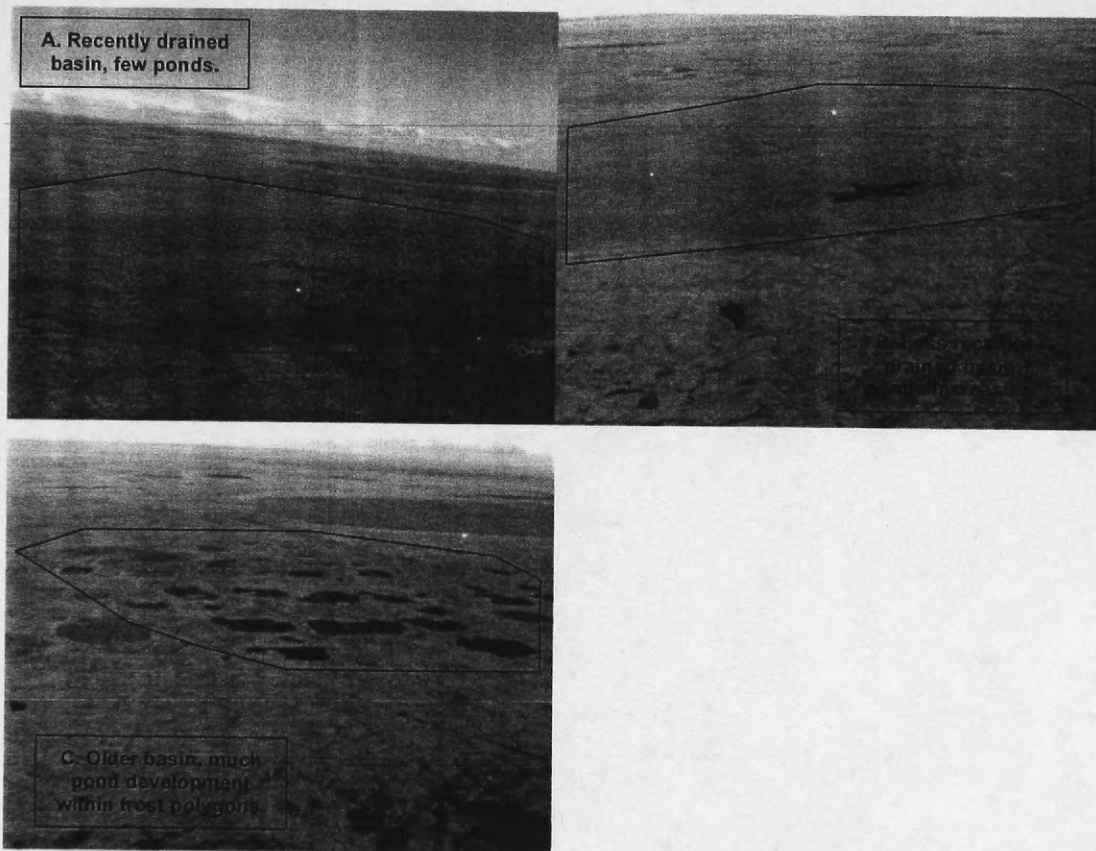


**Figure 6. Example drained thaw lake basins at varying stages of development.**

The accumulation of organic matter within DTLB is of primary interest to this research. Recent studies have shown that peatlands may provide archives of mercury deposition in the Arctic (Roos-Baraclough and Shoty, 2003; Givélet et al., 2004a; Shoty et al., 2005). Lodenius (1983) demonstrated that peat strongly complexes oxidized mercury and extensive research has been conducted using evidence from peat bogs to reconstruct past mercury deposition (Pheiffer-Madsen, 1981, Jensen and Jensen, 1991, Norton et al., 1997, Benoit et al., 1998, Martinez-Cortizas et al., 1999, Biester et al., 2002, Bindler, 2003).

However, until now, no study has been conducted with the intention of quantifying historic mercury deposition along the northern coast of Alaska.

In addition to fieldwork conducted in the Barrow area, samples were collected near Atkasuk, Alaska and Fairbanks, Alaska. The landscape near Atkasuk is similar to that of the Barrow vicinity though it is farther inland. Tundra vegetation is the dominant fauna, frost polygons are well developed, and ovate lakes are present in abundance. Fairbanks, 800 km south of Barrow, is warmer (mean daily maximum: 3.6 °C, mean daily minimum -7.1 °C) and wetter (300 mm of total precipitation with 1,453 mm in snow) than Barrow (National Climate Data Center). Samples were taken in the Caribou Poker Creek Research Watershed in the Chatanika National Forest at two sites where peat was present. The first site was a thermokarst area near a small stream; vegetation consisted of mixed shrubs, deciduous and coniferous trees with spongy organic soil overlying mineral rich sediments. The second site was near (~3m) a thermokarst pond in similar vegetation and soil to the first site. The topography of the two sites was dissimilar. The first site sloped at a gradient of approximately 8% while the site near the pond was almost flat.



## Methods

Approximately 130 tundra soil cores were collected in August of 2005 in the area east-southeast of Barrow, AK. Soil samples were sampled following one of two different procedures. At several sampling sites we hammered plastic tubing (acid-cleaned PVC or butyrate) into the ground to the depth of the permafrost (approximately 30 cm) and extracted soil cores. Compaction of soils was unavoidable with this method so we used an alternative method at most locations. Blocks of tundra soil spanning the depth of the active layer were cut from the center of shovel-excavated plugs with a stainless steel knife. The soil samples, in blocks measuring roughly 5 cm x 5 cm x 30 cm, were described in the field, wrapped in waxed coated paper, labeled, and placed in plastic bags for transport back to the Barrow Arctic Science Consortium (BASC). Descriptions of each core are found in Appendix A.

Upon the cessation of daily fieldwork the soil samples were placed in a freezer. The frozen samples were shipped in coolers to the Department of Geological Sciences at the University of Michigan where they were placed in a freezer at -10° C. Subsequent laboratory methods were modified from previously established protocols for handling and preparing peat samples for mercury analysis (Roos-Barraclough et al., 2002b; Givelet et al., 2004b).

Frozen cores were sub-sampled in the laboratory using a stainless-steel band saw (Cabela's Commercial Grade Butcher Band Saw). The cores were first cut lengthwise into two halves. One half of each core was returned to the freezer as an archive while the other was sectioned for analysis. Cores were laid flat on the band saw's cutting bench and cuts perpendicular to the cores' length were made at each centimeter along the cores' length. The sectioning process resulting cross-sectioned cores with each cross-section piece a rectangular prism measuring approximately 1 cm in height. Work always progressed from the bottom to the top of the core to minimize contact between the lower and upper layers that presumably contain lower and higher levels of mercury respectively. Vegetation was removed from the top of each core and was separated from soil samples. To create replicate samples the cross-section pieces were cut in half. Each half was then squared with an acid-washed sturdy serrated plastic knife on a polyethylene cutting board. Next, each sample was excoriated with plastic scraping tools to remove contamination potentially generated during the cutting process. The x, y, and z dimensions of each subsample was measured to the nearest tenth of a centimeter and placed in pre-labeled, pre-weighed Whirl-Pak plastic bags. One piece per measured depth was designated for mercury analysis while its complement was placed in frozen storage for future analyses. After dissection of each core, the saw assembly and work area were cleaned with distilled water and then wiped with alcohol. The stainless steel saw blade was removed, cleaned

thoroughly with soapy hot water, and rinsed with distilled water. The plastic knife, plastic scrapers and plastic cutting board were cleaned in a similar manner with an additional acid rinse step added to ensure removal of mercury contamination.

The core pieces destined for mercury analysis were placed frozen into a freeze dryer (Virtis Freezemobile 12SL) where they were freeze-dried in a vacuum (lyophilized) for a minimum of 24 hours at  $-55^{\circ}\text{C}$ . Afterwards their dry masses were recorded. Dry-weight bulk density was determined by dividing the dry mass (g) of each subsample by its volume ( $\text{cm}^3$ ), the product of its x, y, and z dimensions measured when the piece was wet and frozen. Moisture content (%  $\text{H}_2\text{O}$  m/m) was calculated by dividing the difference in wet versus dry sample mass by the original wet sample mass.

A Spex 8000M Mixer/Mill was used to homogenize the freeze-dried samples. The dried sub-samples were placed in an alumina ceramic vial containing two alumina ceramic balls and milled for one minute. The pulverizing action of the mixer/mill resulted in powdered samples. The homogenized samples were returned to their original Whirl-Pak bags. Between samples the ceramic vials and ceramic balls were scraped clean, washed in soapy water, rinsed with distilled water, and wiped with alcohol.

Ash content (the inorganic fraction of the soil) was determined by loss on ignition (LOI) analysis of selected dried, homogenized samples. Aliquots of pre-weighed samples were heated at  $550^{\circ}\text{C}$  in a muffle furnace for approximately 4 hours to completely combust organic carbon. Samples were then post-weighed. The sample mass remaining after combustion was divided by the original sample mass to determine % ash content. The ash content per volume of sample was also determined. First, the aliquot volume was determined by dividing the aliquot mass by its dry bulk density. Next, the post-combustion mass of each aliquot was divided by aliquot volume.

Mercury concentrations were determined using a Nippon Instruments MA-2000 mercury analyzer. Within the MA-2000, solid aliquots are combusted at  $800^{\circ}\text{C}$  to drive off mercury vapor. The  $\text{Hg}^0$  is collected on an analytical gold trap as a gold-mercury amalgam. The gold trap is subsequently heated to  $640^{\circ}\text{C}$  driving off the mercury vapor. Mercury concentrations are quantified by atomic absorption spectrometry (AAS). Calibration curves were generated daily by serially diluting a Nippon Instruments 1001 mg/L ( $\text{HgCl}_2$ ) mercury standard. Accuracy was determined by analyzing at least one check standard per eight samples. Check standards were prepared from a Nippon Instruments liquid mercury standard. The detection limit ( $3\sigma$  above the average of the blank values) was 0.15 ng Hg. This translates into 1.46 ng/g during the analysis of a 100 mg sample. See Appendix B for a complete description of the solid sample

mercury analysis procedure used in this study. Mercury concentration was calculated using the MA-2000 software and was determined by finding the quotient of measured mercury (ng) and the corresponding aliquot mass (g). Total mercury content (ng Hg/cm<sup>3</sup>) was calculated by multiplying mercury concentration values (ng Hg/g) of each subsample by the dry bulk density (g/cm<sup>3</sup>).

The ages of the oldest organic matter contained within each core for three of the ten cores (cores B2, B4, and B5) used in this study were taken from published data (Hinkel et al., 2003). To attain the radiocarbon dates Hinkel et al. (2003) first identified the organic material-lacustrine material boundary that marks the beginning of peat accumulation in each DTLB. Organic material immediately above the boundary was picked from bulk material and dated for Carbon-14 using Accelerator Mass Spectrometry (AMS). The age of one of the ten cores (core B6) comes from Brown et al. (1980) who state that the thaw lake that once covered the core B6 sampling location was drained in 1950. The ages of five of the ten cores (cores B1, B3, A1, A2, F2) were determined via AMS radiocarbon dating at the National Ocean Sciences Accelerator Mass Spectrometry (NOSAMS) facility at the Woods Hole Oceanographic Institution in Woods Hole, MA. In order to select organic matter to be dated for radiocarbon, under a dissecting scope organic matter was carefully picked from freeze-dried subsamples taken from the bottom of the organic layer of cores B1, B3, A1, and A2. Only homogenized material remained of core F2 and samples of this material was sent away for dating. Only core F1 of the ten cores was not dated. Because only homogenized material remained of core F1 when material was to be sent away for dating and homogenized material yields questionable radiocarbon dates given the chance for modern C-14 to intermix with older C-14, core F1 organic material was not dated. In this light, radiocarbon dates for core F2 must be viewed as first order estimates. A description of the protocols and procedures used at the NOSAMS facility is found in Appendix C.

## Results

### *Organic Layer Thickness*

The thickness of organic matter deposited after thaw lake drainage was measured in each core. The organic layer consists of peat and organic matter in various stages of decay with occasional intermixed silty layers. Generally speaking, the thickness of the organic layer increased with core age. Lacustrine sediments deposited by thaw lakes and found beneath the organic layer are composed largely of silt and clay with intermixed organics. The organic layer thickness for each core is found in table 1.

Core Name (abbreviated)	Core Name (field)	Location		Field Age Classification	Age of Oldest Organics	Organic Layer Thickness (cm)
B1	05BS41A	71.217° N	156.485° W	Ancient	3700 ±130 <sup>2a</sup>	22
B2	1C	71.203° N	156.531° W	Ancient	2260 ±60 <sup>2b</sup>	35*
B3	L13	no data	no data	Ancient?	3940 ±190 <sup>2a</sup>	≥27
B4	3C	no data	no data	Old	590 ±50 <sup>2b</sup>	8
B5	05BS43A	71.225° N	165.477° W	Young	<55 <sup>2b</sup>	4
B6	05BS37B	71.270° N	156.649° W	Young	56 <sup>2c</sup>	8
A1	05BS32C (ATQ)	70.455° N	157.387° W	Medium to Old?	1430 ±120 <sup>2a</sup>	≥20
A2	05BS34B (ATQ)	70.457° N	157.371° W	Young to Medium?	590 ±95 <sup>2a</sup>	8
F1	05FS01A	65.155° N	147.492° W	N/a	no data	6
F2	05FS02A	65.163° N	147.499° W	N/a	<55 <sup>2a</sup>	7

**Table 1. Core names, locations, oldest organic material ages, and organic layer thicknesses.**

1- Field ages from Hinkel et al. (2003); question marks indicate basins not classified by Hinkel et al. (2003), field ages of these cores were estimated in the course of this work.

2a- Data from soil samples taken during 2005 Alaska field work, profile ages (C-14 dating) from NOSAMS; 2b- ages (C-14 dating) from Hinkle et al. (2003); 2c- age (based upon the known date of basin drainage) from Brown et al., 1980

### *pH*

The pH of standing water on tundra soils was measured in the Barrow area in the Mayoak drainage near core collection sites on 8/13/05. A pH meter was lowered into small pools of standing water that had collected between frost polygons. The waters exhibited a pH range of 4.6 to 5.3.

### *Moisture Content*

The six soil cores from Barrow area DTLB can be sorted into two groups based on moisture content. The three older cores (B1, B2, and B3) are wettest near the surface then show variability in moisture content

with depth through the organic layer while the three younger cores (B4, B5, and B6) show consistently decreasing moisture content with depth. Atqasuk area cores A1 and A2 show a similar moisture content pattern to the three younger cores from the Barrow area. Moisture content is elevated near the surface and decreases with depth. The average moisture content for the top three cm of the six Barrow cores is 80% while the average for the top three cm of the two Atqasuk cores is 77%. Fairbanks area cores F1 and F2 are drier than the Arctic cores; the average moisture content for the top 3 cm is 53%. These two cores show generally decreasing moisture content with depth, however core F1 shows a second soil moisture peak at approximately 30 cm. Moisture content figures for each core are found in Appendix D.

When possible moisture content analyses were performed for multiple subsamples taken at the same depth within a core. The mean and standard deviation for these analyses was determined for each subsample. Relative standard deviation (RSD), the quotient of the standard deviation and the mean expressed as a percent, was then calculated for each subsample. The average relative standard deviation was determined for each core where replicate moisture content analyses were performed. The low RSD values for moisture content indicate consistency in moisture content measurements

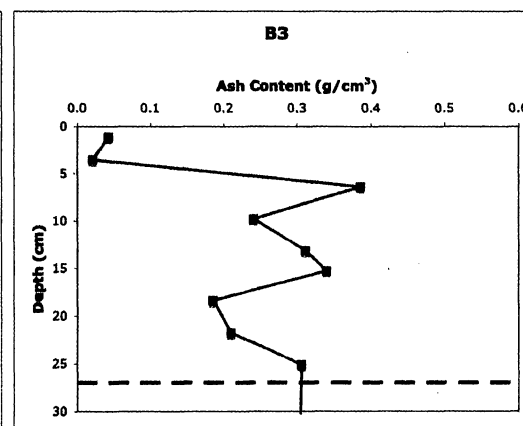
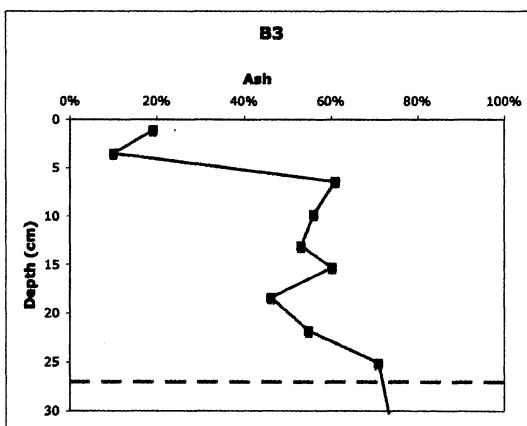
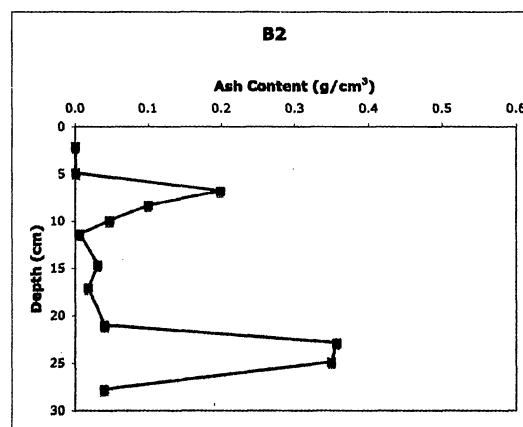
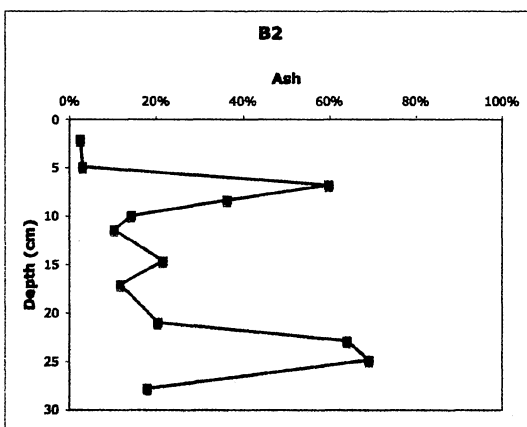
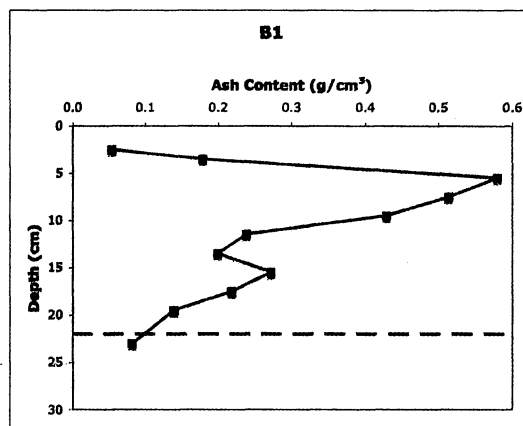
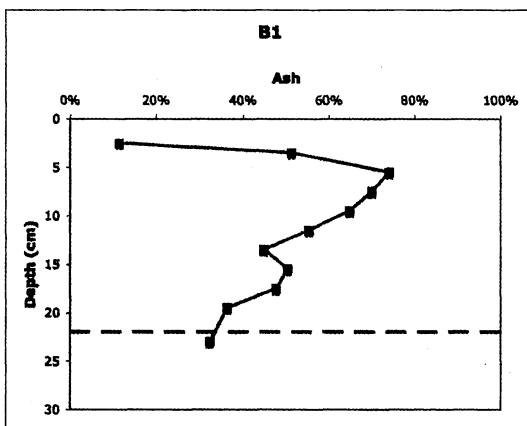
Core:	Moisture Content RSD:	n=
B2	3%	28
B3	7%	31
B4	1%	3
B6	6%	14
A1	3%	11
A2	2%	6

**Table 2. Moisture content measurement error.**

### *Ash Content*

Cores B1 and B2 have very low ash content in terms of both % ash and grams ash per cm<sup>3</sup> near the surface but contain a zone enriched in ash in the upper 10 cm. Core B2 shows a second layer elevated in ash content at a depth of approximately 25 cm. Cores B3, B4, and A1 contain low amounts of ash near the surface but show increasing ash contents with depth. Core B4 has the highest measured ash content of any of the tundra cores. From a depth of 8 cm to 20 cm in a layer described as medium brown peaty silt core B4 has an average of 1.03 g ash/cm<sup>3</sup>. Cores B3 and A1 show increasing ash content from the near-surface peat to the sub-surface organic-rich soil. Below the organic layer these cores show an ash content of approximately 60% by percent mass and contain between 0.2 and 0.4 g ash per cm<sup>3</sup>. Core A2 shows rapidly increasing ash content with depth. Ash content analyses for the two cores taken from ‘young’

DTLB, cores B5 and B6, was not carried out due to a paucity of remaining sample after mercury analysis. Ash content of the Fairbanks area cores is very low in terms of both percent ash and grams of ash per cm<sup>3</sup> in the upper 6 cm but transitions rapidly to elevated levels at depth.



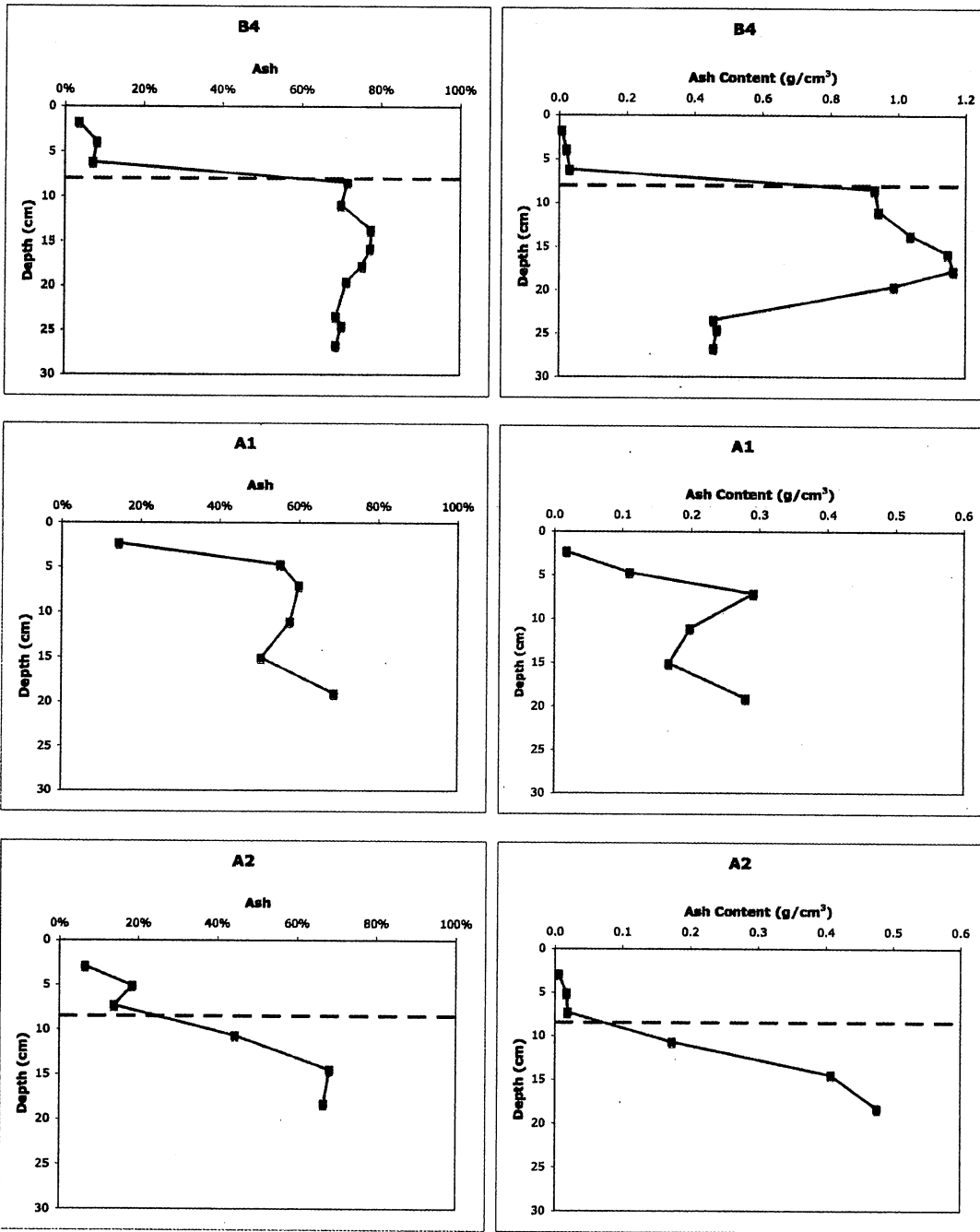


Figure 7a. Ash content in Barrow and Atkasuk area soil cores. Note the dashed horizontal line represents the organic-rich, mineral-rich sediment interface. Where the dashed line is absent the core did not reach the depth of the interface. Also note the change in scale for core B4 to accommodate its high ash content ( $\text{g}/\text{cm}^3$ ).

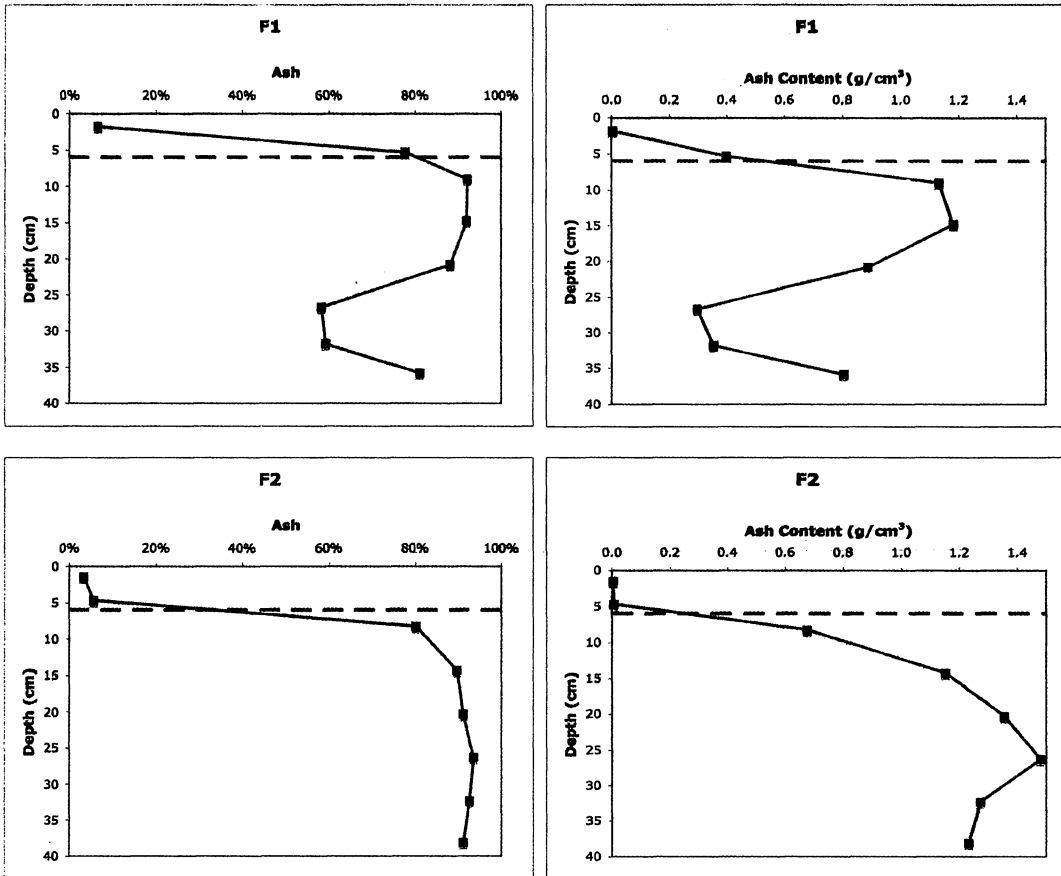
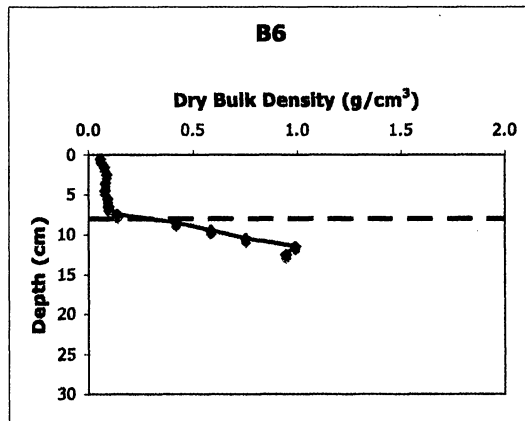
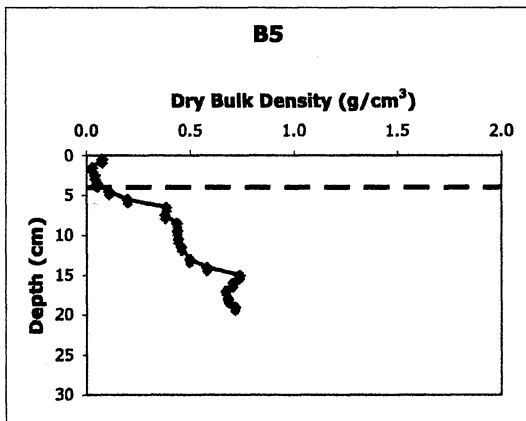
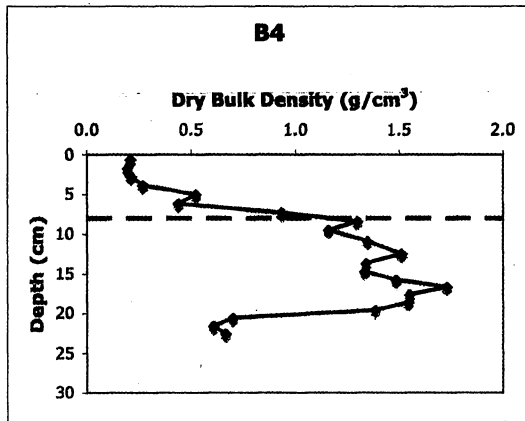
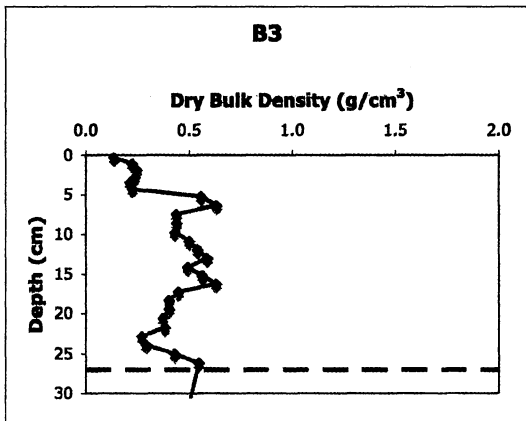
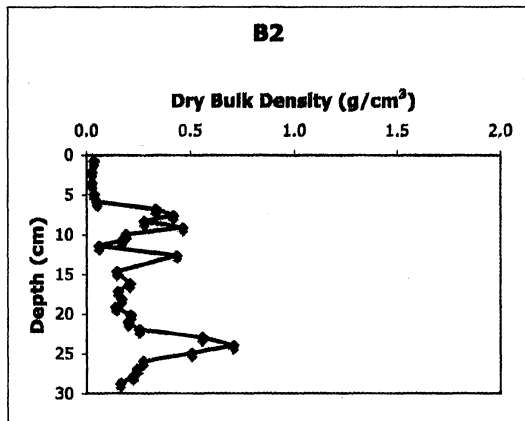
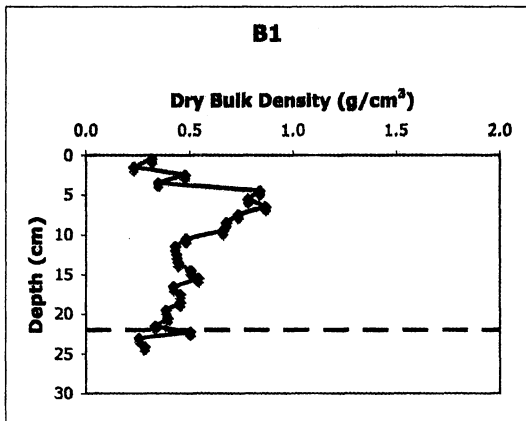


Figure 7b. Ash content in Fairbanks area soil cores. Note the dashed horizontal line represents the organic-rich, mineral-rich sediment interface.

### *Bulk Density*

Barrow area cores B5 and B6 from 'young' DTLB show similar bulk density profiles. Each contains a thin layer of low-density organic material near the surface then transitions to denser lacustrine sediments below. Like the younger Barrow area cores the four older cores (B1, B2, B3, and B4) contain low-density material near the surface and are denser below, but unlike their younger counterparts show more variability in density with depth. For the Barrow area cores, the organic layer has a dry bulk density range of 0.02 to 0.87 g/cm<sup>3</sup> with a mean of 0.33 g/cm<sup>3</sup>. Below the organic layer the mean bulk density increases to 0.82 g/cm<sup>3</sup> with a range of 0.11 to 1.73 g/cm<sup>3</sup>. Atkasuk core A1 displays a similar profile to that seen in Barrow area cores B2 and B3 while core A2 exhibits a bulk density profile comparable to that seen in 'young' core B6. The Fairbanks area cores show low dry bulk density values in the upper 5 cm and transition to denser, mineral-rich sediments beginning between 5 cm and 10 cm.





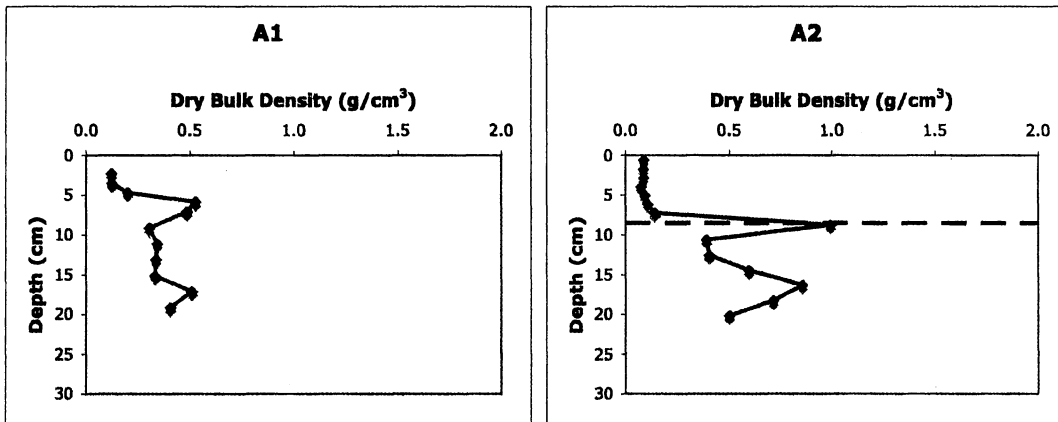


Figure 8a. Dry bulk density measurements in Barrow and Atkasuk area soil cores. Note the dashed horizontal line represents the organic-rich, mineral-rich sediment interface. Where the dashed line is absent the core did not reach the depth of the interface.

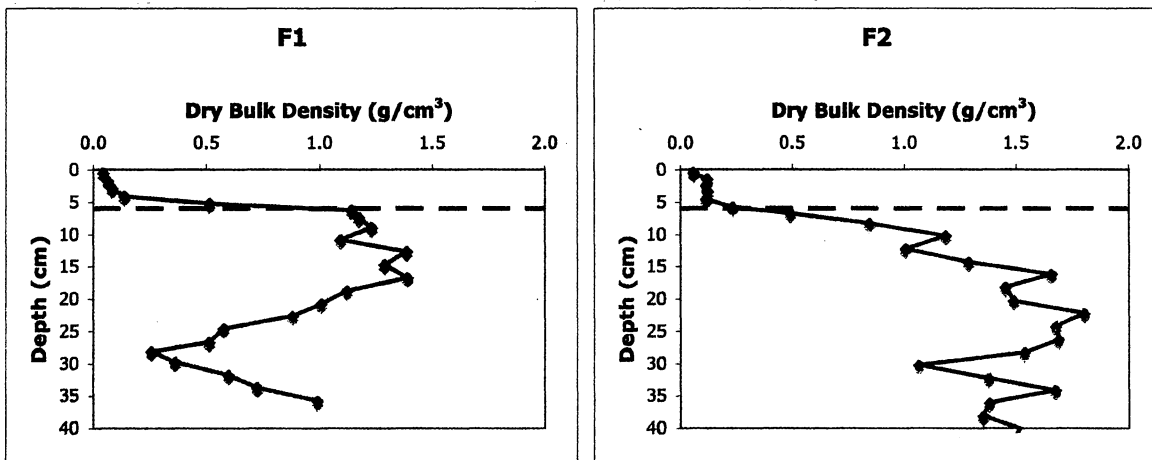


Figure 8b. Dry bulk density measurements for Fairbanks area soil cores. Note the dashed horizontal line represents the organic-rich, mineral-rich sediment interface.

When multiple subsamples were taken at a given core depth, replicate bulk density analyses were performed. The mean and standard deviation with respect to bulk density was then determined. Relative standard deviation (RSD), the quotient of the standard deviation and the mean expressed as a percent, was calculated for each subsample. The average relative standard deviation was then determined for each core where replicate bulk density analyses were performed. The error values are high probably due to inaccuracies involved in measuring the x, y, and z dimensions of the squared sub-samples. The three dimensions were measured to determine each sub-sample's volume, but because the sub-samples rarely had perfectly squared edges some estimation of length was involved in each measurement.

Core:	Bulk Density RSD:	n=
B2	14%	28
B3	21%	30
B4	1%	3
B6	20%	13
A1	13%	11
A2	24%	6

**Table 3. Bulk density measurement error.**

### *Mercury Concentration*

Mercury concentrations of subsamples from the six Barrow area cores range from 647 ng Hg/g to 39.8 ng Hg/g (see table 4). Cores B1, B2, B3, and B4 taken from older DTLB show maximum mercury concentrations near the surface and minimum concentrations at between 14 and 23 cm. The mercury concentration profiles from the two Atqasuk area cores are similar in shape to Barrow area cores B1, B2, B3, and B4. Cores A1 and A2 show maximum mercury concentration values near the surface with minima at depth. However, maximum values for cores A1 are less than are observed for Barrow area cores B1, B2, B3, and B4. As such, a qualifying point must be made at this time. It was discovered during mercury analyses that the Nippon Instruments MA-2000 produced higher mercury (increases up to 100%) measurements when samples were analyzed in a pattern of sample-purge-sample versus a pattern of sample-sample-sample. The MA-2000 is programmed to cleanse the gold trap after each sample run, but due to the organic-rich nature of these peaty samples, additional cleansing was necessary to attain more accurate mercury concentrations. As seen in figure 9, mercury analysis of core B1 yielded higher concentrations when purges were inserted between sample analyses. While conducting repeat mercury analyses with the addition of the purge step, samples from cores A1 and A2 were accidentally omitted. The authentic mercury concentrations for subsamples within these cores must be assumed to be higher than is reported above, possibly in the mercury concentration range of the four older Barrow area cores.

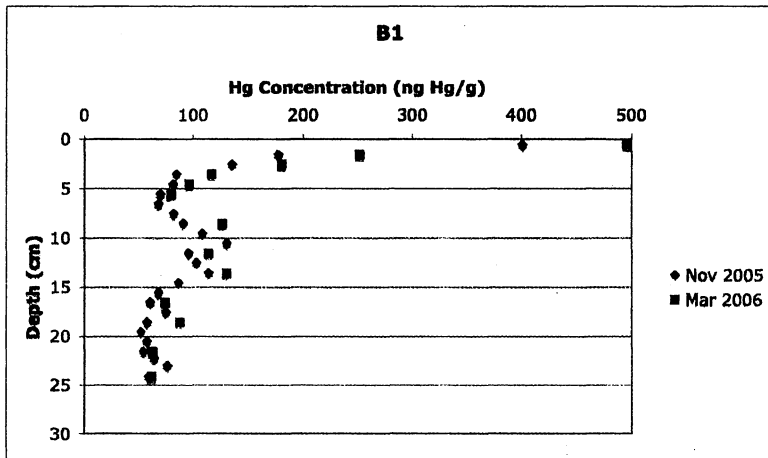


**Figure 9. Mercury analysis of core B1 with and without an additional purge step to purify the mercury analyzer's analytical gold trap. Note increased mercury concentrations especially in the highly organic upper layers of the profile. Replicate samples analyzed in March of 2006 were run with the additional purge while samples analyzed in November of 2005 were run without the additional purge step.**

Cores B5 and B6 from 'young' DTLB have similar mercury concentration profiles. They each show minimum mercury concentrations near the surface with maximum concentrations of approximately 100 ng Hg/g between 5 and 10 cm below the surface. Mercury concentration profiles for the two Fairbanks area cores show increasing concentrations with depth to approximately 6 cm. Below 6 cm core F2 shows consistent mercury concentrations while core F1 contains rising mercury concentrations at a depth of approximately 25 cm.

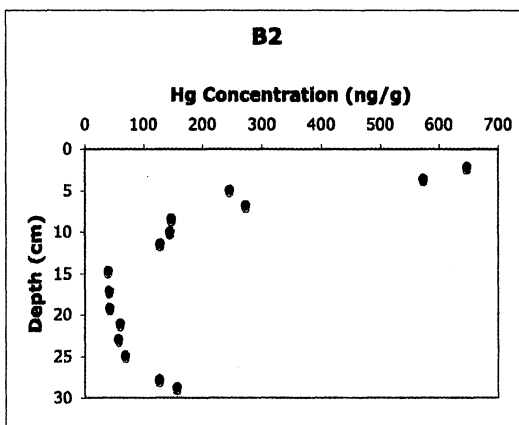
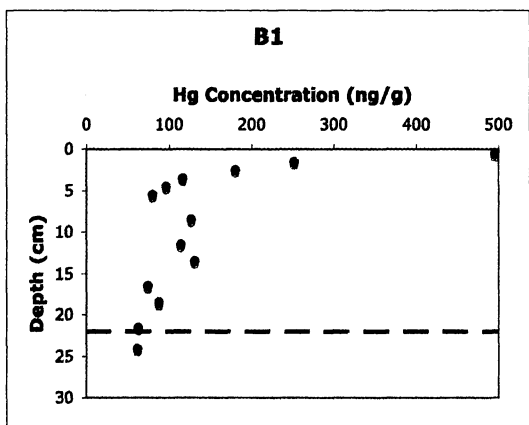
Core	Maximum Hg Conc. (ng/g)	Depth (cm)	Minimum Hg Conc. (ng/g)	Depth (cm)
B1	495	0.5	61.9	24
B2	647	2.0	39.8	15
B3	364	0.5	62.7	23
B4	468	4.0	58.0	16
B5	128	4.5	46.4	0.5
B6	93.8	8.5	46.9	1.5
A1	360	3.5	71.4	13
A2	264	2.0	75.4	15
F1	104	30	35.2	17
F2	137	6.0	47.7	22

**Table 4. Minimum and maximum mercury concentrations by soil core.**

Precision for mercury analyses was measured by analyzing replicate samples (n= 33). An average RSD, the average variation among replicate analyses for a given sample, of 6% was calculated (table 5). As previously mentioned, accuracy was verified by analyzing standards of known concentration at regular intervals. An average RSD, the average difference between expected and measured mercury content, of 7% was calculated for the check standards which translates into  $\pm 0.7$  ng Hg when analyzing a 10 ng Hg/g check standard.

Core	Mercury Concentration Measurement Error (%)	n=
B1	2	1
B2	12	5
B3	5	10
B4	7	3
B5	0	1
B6	3	1
A1	2	2
A2	2	3
F1	2	3
F2	7	4
All Cores	6	33

Table 5. Mercury concentration analysis precision, results of replicate mercury analyses.



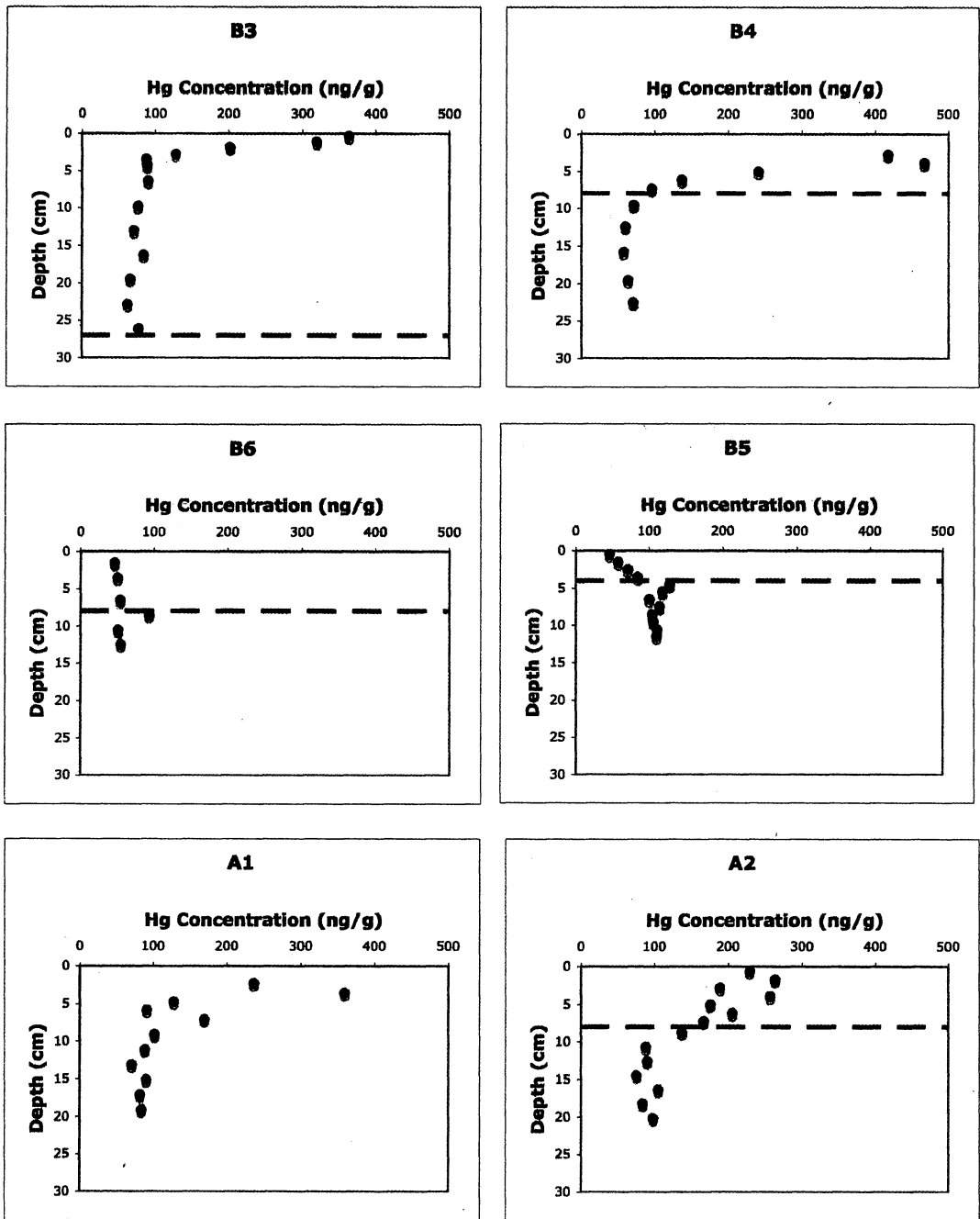


Figure 10a. Barrow and Atqasuk area soil profile mercury concentrations. Note the dashed horizontal line represents the organic-rich, mineral-rich sediment interface. Where the dashed line is absent the core did not reach the depth of the interface.

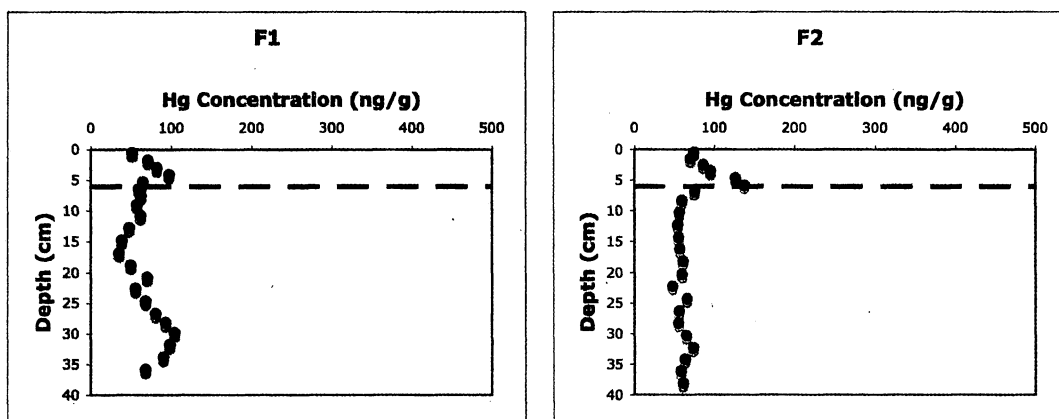


Figure 10b. Fairbanks area soil profile mercury concentrations. Note the dashed horizontal line represents the organic-rich, mineral-rich sediment interface.

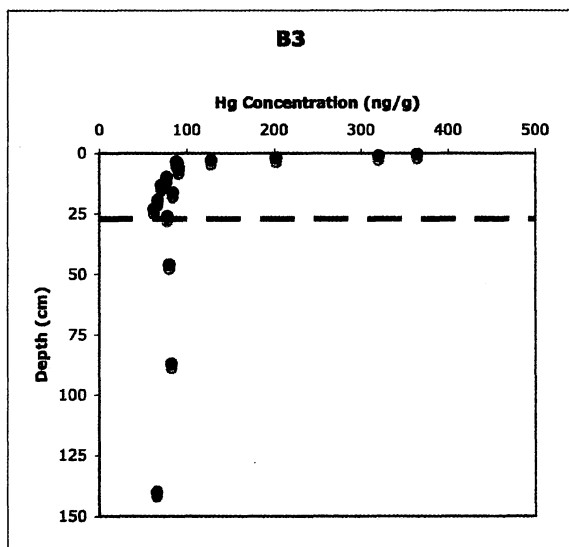


Figure 10c. Extended mercury concentration vertical profile of core B3. Note the dashed horizontal line represents the organic-rich, mineral-rich sediment interface.

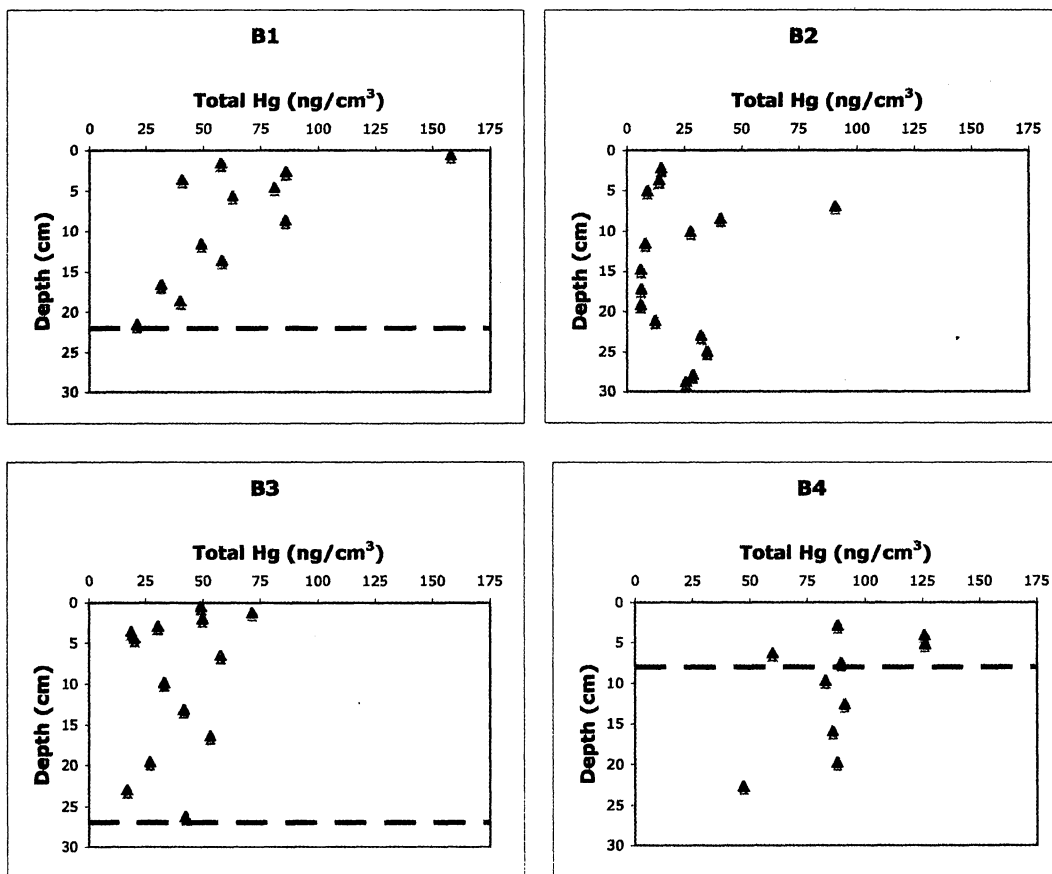
### *Total Mercury Content*

Within each core sub-sample total mercury content ( $\text{ng Hg/cm}^3$ ) was calculated as the product of mercury concentration ( $\text{ng Hg/g}$ ) and dry bulk density ( $\text{g/cm}^3$ ). Cores B1, B3, B4, and A1 show decreasing or relatively stable total mercury content profiles with depth while Barrow area cores B5, B6, Atkasuk area core A2 and the two Fairbanks area cores F1 and F2 show generally increasing values of total mercury content with depth. Core B2 is anomalous in that it contains a zone of high total mercury content between 5 and 10 cm with lower total mercury content above and below this zone.

Error in total mercury content is reported as the sum of the error for bulk density and mercury concentration measurements. Results of error calculations are reported below for those cores where replicate subsamples were taken at various depths upon which replicate bulk density analyses were performed. The high error values for total mercury are largely due to the elevated error in bulk density measurements.

Core:	Error in Total Hg Content (ng/cm <sup>3</sup> ):
B2	± 26%
B3	± 26%
B4	± 8%
A1	± 15%
A2	± 27%

Table 6. Total mercury content calculation error (the sum of bulk density and mercury concentration measurement errors).





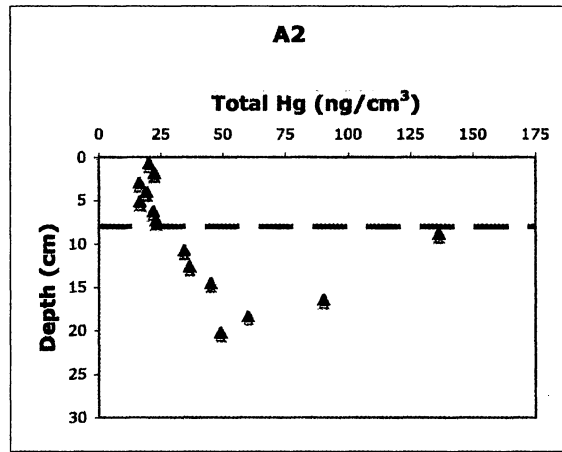
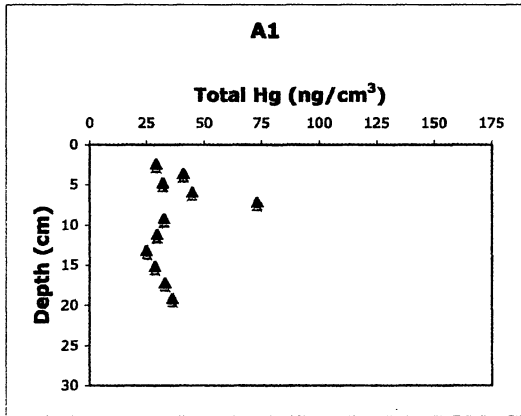
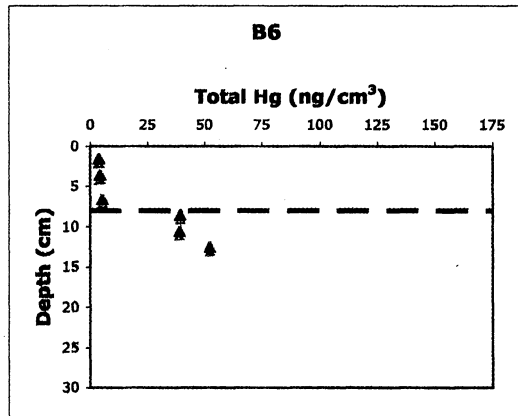
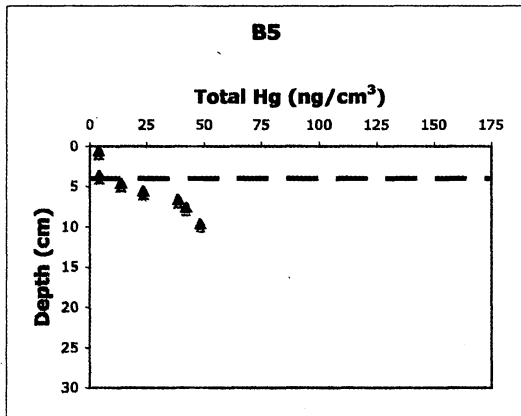


Figure 11a. Barrow and Atkasuk area soil core total mercury calculation results in units of  $\text{ng Hg}/\text{cm}^3$ . Note the dashed horizontal line represents the organic-rich, mineral-rich sediment interface. Where the dashed line is absent the core did not reach the depth of the interface.

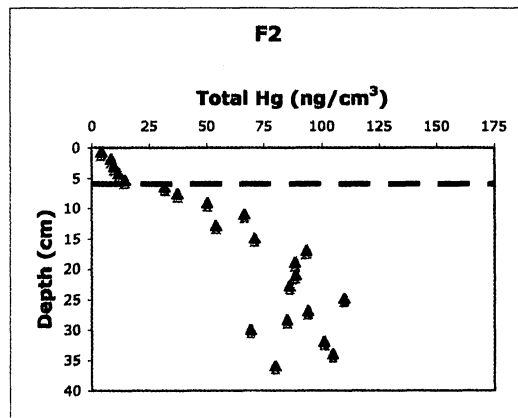
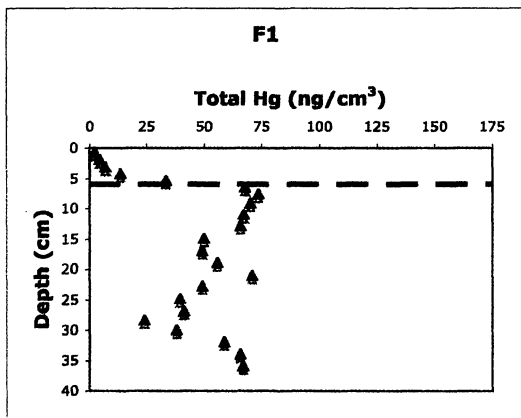


Figure 11b. Fairbanks area soil core total mercury measurements by  $\text{ng Hg}/\text{cm}^3$  and  $\text{ng Hg}/\text{g ash}$ . Note the dashed horizontal line represents the organic-rich, mineral-rich sediment interface.

Table 6 displays preliminary total mercury results for peat profiles taken in adjacent wet and dry areas near Barrow. Wet (low-lying) areas appear to concentrate mercury. This likely happens during snowmelt as mercury moves laterally across the tundra sorbed to dissolved organic material. By limiting sampling to elevated areas only a more accurate estimate of atmospherically deposited mercury is obtained.

B5 (wet site)	45.5
B5 (dry site)	56.7
B4 (wet site)	72.8
B4 (dry site)	39.6
B3 (wet site)	48.5
B3 (dry site)	11.0

**Table 7. Wet vs. dry site mercury contents. Note that 'Basin' refers to DTLB names given in Hinkel et al. (2003).**

## Discussion

The driving questions for this work will now be examined in light of the results presented above. Questions regarding changing mercury concentrations within soil profiles, whether these data corroborate reports of increasing mercury deposition across the Arctic, the spatial and temporal extent of MDE, and the role of tundra soils in the local mercury cycle will be examined. The questions will be addressed by way of discussion of the physical characteristics of Alaskan tundra soils and the limiting factors in their utility as geochemical archives, discussion of mercury concentrations relative to soil mass, volume and ash content, and finally through discussion of mercury flux calculations and the relevance of these calculations to the nature of MDE.

### *Physical Characteristics of Tundra Soils in Comparison to Peat Bogs*

As previously mentioned, peat bogs have been thoroughly studied as archives of mercury deposition. The tundra soils of northern Alaska are considerably more variable in composition but yet bear similarities, especially in the upper portions of their profiles, to peat bogs. The two depositional environments are especially similar in abundances of organic material and in that mercury is supplied to each via atmospheric inputs. Because of these similarities the tundra soils presented here are likely to record mercury deposition in a similar manner to peat bogs.

Alaskan tundra soils are similar to peat bogs in terms of pH. As there is no input of ground water laden with dissolved bicarbonate to ombrotrophic peat bogs, un-neutralized organic acids accumulate resulting in acidic conditions and a pH of 3.7 to 4.2 (Shotyk, 1988). Standing water near coring sites on the Arctic tundra is slightly less acidic than peat bogs (4.6 to 5.3). Soils in the Barrow area have a higher carbonate component than would be found in a true bog setting (FitzPatrick, 1997).

Tundra soils and peat bogs also have similar moisture content. Peat tends to be 90-95% water by weight (Shotyk, 1988). The upper layer of these tundra soils averages 77% moisture content over the top 3 cm of the cores and 70% over the entire span of the organic layer (Appendix A). Of consideration, however, is that water was lost during sampling and handling of the soil cores. In situ moisture content measurements would probably have yielded higher values than are presented here, measurements more similar to those seen in peat bogs. Additionally, the time of year the tundra soils are sampled can significantly affect moisture content. As the active layer thaws, melt water drains laterally along the gentle slope of the tundra or is lost by evapotranspiration. Evapotranspiration increases in intensity through the summer

months and additional soil water is lost to the atmosphere during that time (Ochelle et al., 1997). Had the tundra soils been sampled soon after snowmelt, moisture content would have been more similar to that of peat bogs. After organic matter is deposited on the tundra it is compressed during additional deposition of organic material from above. Organic matter also decays over time further compacting the soil. Soil compaction results in decreasing porosity (ratio of the volume of void space to the total volume), a decreased ability to retain moisture. Compaction is responsible for the low moisture content (40-60%) at depth in the tundra soil cores. Recently deposited peat has a porosity of 80 to 97% (Hogan, 2005).

Peat is defined as material having an ash content, the percentage of mineral matter in the soil by mass, of <25% (Shotyk, 1988). As such, these tundra soil cores are similar to peat bogs in the top 3 to 7 cm of each core (figure 7a). Below the topmost organic layer there generally exists compressed organic-rich soil containing approximately 60% mineral matter. The decomposition of organic matter increases relative ash content within tundra soils with age. It is assumed that despite the decomposition of organic matter, mercury is retained in the profile not necessarily sorbed to peat as in the peat bog studies, but sorbed to the humic substances left behind after the partial decomposition of organic material. The transition from organic-rich surface material to mineral-rich soil that demarks the transition from thaw lake sediments to DTLB organic accumulation is seen most clearly in the ash content profile of core B4. At a depth of 8 cm the sediments contained within core B4 transition rapidly from dark brown organic-rich peat to medium brown, silty, organic-poor material (Appendix A). Additionally at this point in the profile, as seen in figure 7a, 8a and Appendix D, ash content, bulk density, and moisture content respectively show rapid increases as is expected in a transition from organic to mineral-rich sediments.

Peat has typical dry bulk densities of approximately  $0.1 \text{ g/cm}^3$  (Hillel, 1982). As with ash content, only the uppermost section of the tundra soil cores is similar to peat with denser sediments lying below (figure 8a). For example, the average density in the upper 8 cm of core B4 has an average bulk density of  $0.31 \text{ g/cm}^3$  while the denser mineral-rich soils from 11 cm to 19.6 cm have an average density of  $1.47 \text{ g/cm}^3$ . This latter value is well within the density range for mineral soils of  $1.1 \text{ g/cm}^3$  to  $1.6 \text{ g/cm}^3$  (Hillel, 1982) and reflects the silt-rich nature of the deeper portion of core B4. Cores B2 and B3 have dry bulk density averages of  $0.24 \text{ g/cm}^3$  and  $0.40 \text{ g/cm}^3$  respectively, suggesting that the soils in cores B2 and B3 are the humified remains of previously deposited organic matter and are not the mineral soil seen at depth in core B4. As such, cores B2 and B3 likely preserve the mercury archive in the same manner as peat bogs.

### *The Specter of Cryoturbation*

Within the dynamic permafrost environment cryoturbation must be considered when interpreting mercury concentration profiles of Arctic soils (Givelet et al., 2004a). Common tundra features signifying subsurface disturbances include frost boils and desiccation cracks. Frost boils are thought to result when a patch of bare ground on the tundra lacking the insulation of vegetation stimulates accelerated freezing of the active layer beneath it. Rapid freezing pulls in water from surrounding sediments (cryosuction) causing ice accumulation beneath the original patch of bare ground and, as a result, differential frost heave (vertical lifting) of the boil sediments (Nettleton, 2005). Frost boils can also mix surficial organic matter well into the active layer (Shur et al., 2006). The mixing of thaw lake sediments with organic material laid down in DTLB would limit a core's usefulness because lacustrine sediments do not accumulate mercury in the same manner (via atmospheric inputs) as do the organics that are deposited after thaw lake drainage. Additionally, desiccation cracks form in tundra soils when surface material dries out, loses volume, and pulls apart. Cracking presents the risk that modern day mercury could penetrate into a soil and confound mercury profile interpretations. To minimize the potential complications caused by frost boils and desiccation cracks sampling locations well away from observed frost boils were chosen and surfaces were sought out that presented uniform vegetation cover in order to minimize the chance of collecting desiccated soils.

Despite efforts to avoid cryoturbation complications, Barrow area cores B1 and B2 from 'ancient' DTLB show ash content and bulk density profiles that could indicate the intrusion of lacustrine sediments perhaps due to frost boil action. Such intrusions would limit the usefulness of these cores in this study of mercury deposited in DTLB. Both cores show a peak in ash content and in bulk density at between 5 and 10 cm that might indicate the mixing in of thaw lake sediments with DTLB organics. Core B1 has a dry bulk density average of  $0.49 \text{ g/cm}^3$  but has a curious bulk density peak of  $0.87 \text{ g/cm}^3$  at a depth of 6.5 cm. This peak coincides with ash content of 72% or  $0.55 \text{ g ash/cm}^3$ . While these spurious characteristics give cause for concern, there are a number of explanations for the higher than expected ash content and bulk density levels. At advanced stages of frost polygon development elevated areas such as the rims of low-center polygons gain additional relative elevation as subsurface ice-wedges degrade, causing further subsidence of low areas (FitzPatrick, 1997). The increase in elevation promotes aridity. Elevated areas on the tundra landscape have the least snowpack because the region's high winter winds scour snow from exposed places. They thus receive less moisture during snow melt than do low areas. Also because they are more exposed, high points on frost polygons receive more solar energy and are rapidly snow-free in the spring. This allows the soil to thaw sooner and be exposed to the atmosphere for a greater period of

time promoting oxidation of organic material. As organic matter is oxidized and breaks down to CO<sub>2</sub> the relative abundance of ash increases as soil volume decreases. The basin from which core B1 was taken has a radiocarbon age of 3700 years. Therefore the organic matter within it has had ample time to decompose, possibly causing ash content and bulk density to be elevated near the surface where the core is in most continuous contact with the atmosphere. Considering the bulk density profile from core B4 suggests that desiccation-related decomposition of near-surface organic matter rather than cryogenic disturbances has resulted in the unusually dense horizon at 6.5 cm within core B1. Core B4 contains mineral-rich sediments underlying an 8 cm near-surface organic layer. If the dense material from B4 with bulk density values of 1.2 to 1.7 g/cm<sup>3</sup> is taken to be representative of lacustrine sediments that lie beneath the organic layer in the DTLB then the 0.87 g/cm<sup>3</sup> peak in bulk density from core B1 represents at most a 50-50 mixing of organic material with lacustrine sediments. Furthermore, Oechel et al. (1997) report that tundra near Barrow, Alaska is currently losing carbon to the atmosphere, especially during the summer months, due to an average regional temperature increase of 2° to 4° C over the past several decades. Rising temperatures have resulted in additional carbon dioxide production, as oxidation of organic matter becomes more rapid and decreasing soil moisture content as evapotranspiration increases. The advanced decomposition of core B1 may be symptomatic of the region's changing climate. Furthermore, as seen in other coastal Arctic locations, input of atmospheric aerosols contributes significantly to the composition of tundra soils. (Givelet et al., 2004a). The spike in ash content and bulk density (figures 7a and 8a) within core B1 could result from a temporary increase in the dust deposition regime as recorded in this 3700 year old core. Core B3, of a similar age to core B1, also contains elevated ash content in its upper 10 cm. In the case of core B2 which has an ash content spike at approximately 7 cm (60% ash, 0.20 g ash/cm<sup>3</sup>) the elevated ash content and bulk density values are, as in core B1, possibly the result of cryoturbation and a mixing in of mineral-rich thaw lake sediments. However, the explanation for these values is likely the same as the one offered for core B1 where extensive oxidation of organics due to advanced core age and increasing aridity artificially inflate relative ash content and bulk density. Supporting this notion is the fact that the layer in contention at 7 cm of core B2 has similar ash content in terms of g ash/cm<sup>3</sup> to sediments found throughout the organic layer of core B3 that shows no signs of disturbance. Also, core B2 contains some of the lowest density material sampled (~0.03 g/cm<sup>3</sup>) within its upper 10 cm that amplifies any relative increase in ash content.

### *Mercury Concentration*

The maximum mercury concentration in core B2 (647 ng Hg/g) is higher than reported values for Arctic peat deposits. Published maxima include 498 ng Hg/g from a Faroe Islands peat bog and 76 ng Hg/g from

Bathurst Island, Canada peat hummocks (Shotyk et al., 2005; Givélet et al., 2004). Within northern Alaska reported maximum lake sediment mercury concentrations from research sites near Toolik Lake on Alaska's North Slope range from 330 ng/g to 186 ng/g (Hammerschmidt et al., 2006; Fitzgerald et al., 2005).

The increasing soil mercury concentrations approaching the surface in cores B1, B2, B3, B4, A1 and A2 (figure 10a) likely indicate increasing mercury deposition through time. If mercury loading via the atmosphere were constant through time it would be expected that mercury concentrations would be relatively stable with depth throughout the organic layer. Low-density organic matter at the surface should show similar or lower mercury concentrations by mass to the denser sediments below where mercury is concentrated due to the decomposition of organic matter. In the case of the Alaskan tundra cores, mercury concentrations are three to six times higher near the surface than at depth. Mercury did not accumulate sufficiently within the deeper sediments when they were deposited at the surface to balance the increase in density coincident with decaying organic material. The near-surface bulk density of the tundra soil cores is  $\sim 0.1 \text{ g/cm}^3$  while at depth in the organic layer the density is  $\sim 0.6 \text{ g/cm}^3$ . As such, the deeper organic sediments have undergone a six-fold increase in bulk density due compression coincident with the decay of organic matter. Organic layer mercury concentrations near the surface are  $\sim 300 \text{ ng Hg/g}$  soil while farther down the concentrations decrease to  $\sim 100 \text{ ng Hg/g}$  soil. The product of mercury concentration and bulk density in this case is nanograms of mercury per cubic centimeter; the upper layers of organic matter have accumulated approximately  $30 \text{ ng Hg/cm}^3$  while the lower layers of organic matter have accumulated approximately  $60 \text{ ng Hg/cm}^3$ . However, when the upper portion of the soil cores eventually undergo the six-fold increase in density they will have accumulated approximately  $180 \text{ ng Hg/cm}^3$ , three times the mercury seen presently at depth. Lower mercury concentrations at depth within the cores' organic layer can be interpreted as stemming from a 'natural' background rate of mercury deposition while concentrations near the surface are interpreted as arising from recent, enhanced deposition.

The two younger Barrow area cores (B5 and B6) have not been accumulating organic matter for a substantial period of time; they reveal only a small portion of the region's mercury deposition history. They show a similar peak in mercury concentration between 5 and 10 cm and decreasing mercury concentrations approaching the surface. The mercury profiles from cores B5 and B6 possibly illustrate maximum global mercury deposition within the middle to late 20<sup>th</sup> century and subsequent declines in deposition within the past few decades as reported elsewhere (Shotyk et al., 2005; Schuster et al., 2002). The mercury concentration profile differences between the younger and older tundra soil cores result from

the extremely different accumulation periods they represent. For example, core B5 has accumulated 4 cm of organic matter over the past 55 years whereas core B1 has accumulated 22 cm of organic matter over 3700 years. B1 shows dramatically increasing mercury concentrations near the surface versus lower concentrations at depth while core B5 has simply not been accumulating mercury long enough to show a well-developed concentration profile.

Mercury concentration profiles for the two Fairbanks area cores (figure 10b) are strikingly different from the tundra cores. They show increasing concentrations with depth to approximately 6 cm and relatively consistent mercury concentrations below instead of dramatic increases near the surface. In terms of magnitude, however, mercury concentrations are very similar to those seen at depth (~100 ng Hg/g) in the tundra cores. The cores from the Fairbanks area are similar to the two younger Barrow area cores in that they may not have been accumulating mercury for a long period of time. Like the younger Barrow area cores, cores F1 and F2 do not show dramatic increases in mercury concentration over time. If thermokarst processes (subsidence due to melting permafrost) have only recently begun at the chosen sampling sites, perhaps due to a warming Alaskan climate, the organic matter deposits from these locations, made possible by the subsiding landscape and the wet depressions found there, may be young in age. Cores F1 and F2 have peat deposits of 6 and 7 cm respectively.

#### *Total Mercury Content*

Because total mercury content is defined as the product of bulk density and mercury concentration, maximum mercury content per unit volume (ng Hg/cm<sup>3</sup>) should occur either where atmospheric mercury deposition is large and much mercury accumulates within the low-density organic matter atop the tundra soil profile or where mercury is concentrated in layers of high bulk density where there has been considerable decomposition of organic matter. In comparing the bulk density and total mercury profiles of cores B1, B3, and B4 (figures 8a and 11a) maximum mercury concentrations occur in the top 5 cm of the cores while maximum bulk density is seen between 5 and 10 cm below the surface. Maximum total mercury therefore is not dependent on bulk density maxima implying that mercury content is also not dependent upon mercury focusing as a result of organic matter decomposition but is due to elevated mercury concentrations. Cores B2, A1, and A2 show more similarity between total mercury and bulk density profiles implying that within these cores total mercury maxima result where mercury is concentrated during the process of organic matter decay.



Within cores B5, B6, F1, and F2 total mercury values mirrors bulk density values. Because mercury has not accumulated to a high degree within the soils where these cores were taken bulk density is the dominant factor in determining total mercury.

*Total Accumulated Mercury*

In order to evaluate the relative ages of the tundra soil cores with respect to mercury, total accumulated mercury (ng Hg/cm<sup>2</sup>) within each core from the surface to the organic-rich/mineral-rich sediment interface that marks the transition between DTLB organic material and thaw lake sediments was calculated. Each sub-sample's total mercury content (ng/cm<sup>3</sup>) was multiplied by its thickness (cm) and the products were summed over the depth of accumulated organic matter. Generally speaking, as seen in figure 12, older basins accumulated more mercury with core B1 accumulating the most mercury. Cores B5 and B6 that are about 55 years in age accumulated at least an order of magnitude less mercury than the oldest cores.

Core	Approximate Age of Oldest Organic Material (years)	Approximate Organic Matter Thickness (cm)	Total Organic Layer Hg Accumulation (ng/cm <sup>2</sup> )
B1	3700	22	1330
B2	2260*	≥29	706
B2 (revised)	2260*	35	872
B3	3940	≥27	971
B4	590*	10	767
B5	55*	4	45.2
B6	56**	8	67.8
A1	1430	≥20	693
A2	590	8	141
F1	unknown	6	62.1
F2	55	7	109

**Table 8. Organic layer mercury accumulation.**

\*from Hinkel et al., 2003.

\*\*from Brown et al., 1980

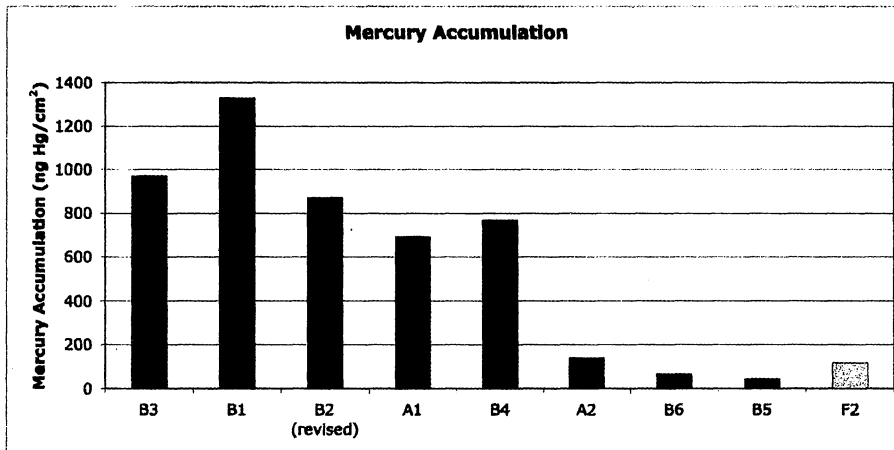


Figure 12. Mercury accumulation (ng Hg/cm<sup>2</sup>) in Alaskan Soil Cores. Cores are arranged from oldest to youngest in order from left to right. Gray bars represent Barrow area cores, black bars represent Atqasuk area cores and the light bar represents core F2 from the Fairbanks area.

Of note in table 8 and figure 12 is the total accumulated mercury value for core B2. When it was taken in August of 2005 core B2 reached only to 29 cm. It was not possible to penetrate deeper given the chosen sampling methods of plug excavation by means of a shovel due to the existence of permafrost at this depth, yet the organic-rich/mineral-rich sediment interface was not yet reached. The organic layer of the basin where core B2 was taken was therefore incompletely sampled. The DTLB from which core B2 was taken is posited to have an organic layer thickness of 35 cm and have been accumulating organic material for 2260 years (Hinkel et al., 2003). Incomplete sampling of the organic layer's depth should result in less than expected mercury accumulation values. This is the case with core B2 that appears to have accumulated less mercury than core B4 despite accumulating mercury 1670 years longer than core B4 (706 vs. 767 ng/cm<sup>2</sup>). By extrapolating the total mercury content (ng/cm<sup>3</sup>) values at the bottom of core B2 an additional 6 cm of mercury accumulation (ng/cm<sup>2</sup>) were added to the originally calculated value. This revised accumulation for core B2 adjusted upward the total mercury accumulated by 166 ng/cm<sup>2</sup> and yields a mercury accumulation value commensurate with core B2's age.

Changes in total accumulated mercury are explained to a high degree ( $r^2 = 0.93$ ) in Barrow area soil cores by changes in core age (figure 13). However, as illustrated by the decreasing slope of the logarithmic function shown in figure 13, the rate of mercury accumulation appears to have increased in recent times. Assuming a constant retention rate for deposited mercury, if mercury accumulation within tundra soils is constant then mercury accumulation plotted against core age would yield a function with a constant slope. As such if mercury accumulation for cores B1, B2, B3 and B4 is plotted against core age the points fall along a linear function as seen in figure 14a. This function describes mercury accumulation in tundra soils of greater than 590 years in age; the slope of the linear function provides a first order estimate as to the

preindustrial background mercury flux to the Alaskan Arctic tundra of  $1.4 \mu\text{g Hg cm}^{-2}\text{yr}^{-1}$ . When mercury accumulation for cores B5 and B6 is plotted against core age (figure 14b) a linear function is generated describing mercury deposition within the last half century. The linear function was best fit through the two data points and assigned a y-intercept value of zero as at time equals zero mercury accumulation would also be zero. Given that the line is drawn through only two data points, the linear function is at best a first order estimate of modern mercury accumulation. The slope of this line, which translates into the modern mercury accumulation rate within tundra soils, is larger than the slope of the line describing background mercury deposition indicating again that mercury accumulation has increased in rate in modern times. From the slope of the linear function in figure 14b a modern mercury flux estimate of  $10.2 \mu\text{g Hg cm}^{-2}\text{yr}^{-1}$  is generated.

Of interest in table 8 and in figures 12 and 13 is that cores A1 and A2 appear to have accumulated less mercury within their organic layers than is observed having accumulated in the organic layer of similarly aged Barrow area DTLB. Both A1 and A2 plot below the mercury accumulation curve in figure 14. Most noticeably is that the oldest organic matter deposited after thaw lake drainage in both Barrow core B4 and Atqasuk core A2 has been C-14 dated as having an age of 590 years before present, yet core B4 has accumulated approximately five and half times more mercury than core A2. However, as was mentioned earlier, the subsamples from core A1 and A2 were analyzed for mercury without the benefit of the gold trap cleaning extra purge step that resulted in operationally increased mercury concentrations in the Barrow area cores. Hence the total accumulated mercury of cores A1 and A2 is very likely underestimated here and being thus the data points for cores A1 and A2 may very well should have plotted on the mercury accumulation curve in figure 14.

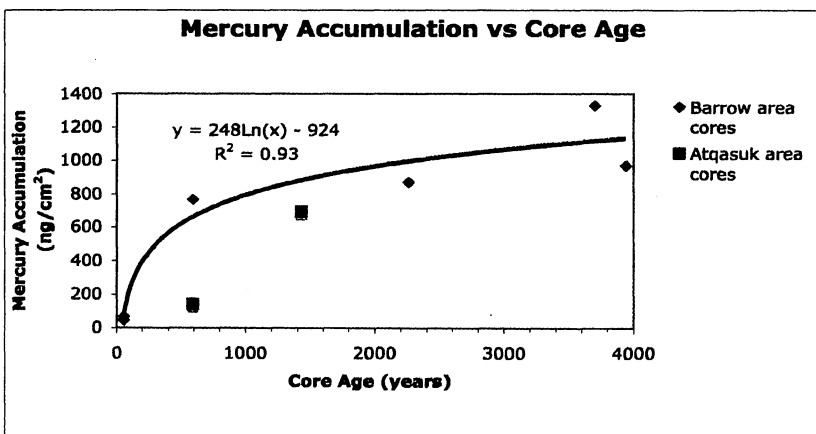


Figure 13. Mercury accumulation versus core age for Alaskan Arctic soil cores. Note that the cores taken inland at Atqasuk appear to have accumulated less mercury over time than the Barrow area cores as seen in that the Atqasuk cores plot below the best-fit logarithmic function plotted through the six Barrow cores.

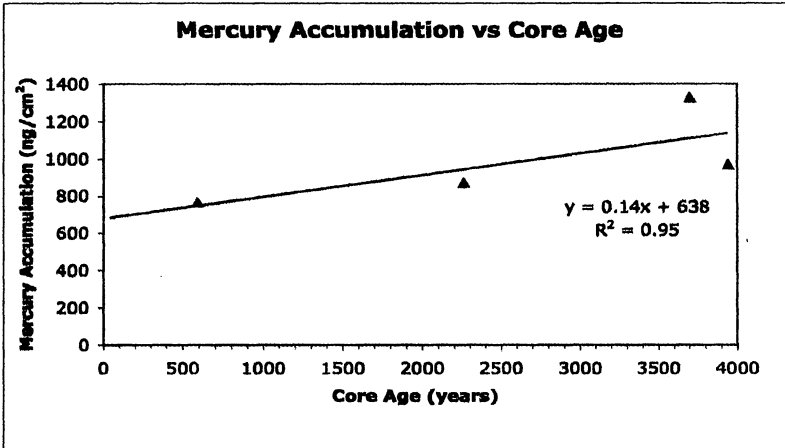


Figure 14a. Mercury accumulation (ng/cm<sup>2</sup>) in four Barrow area soil cores >590 years in age.

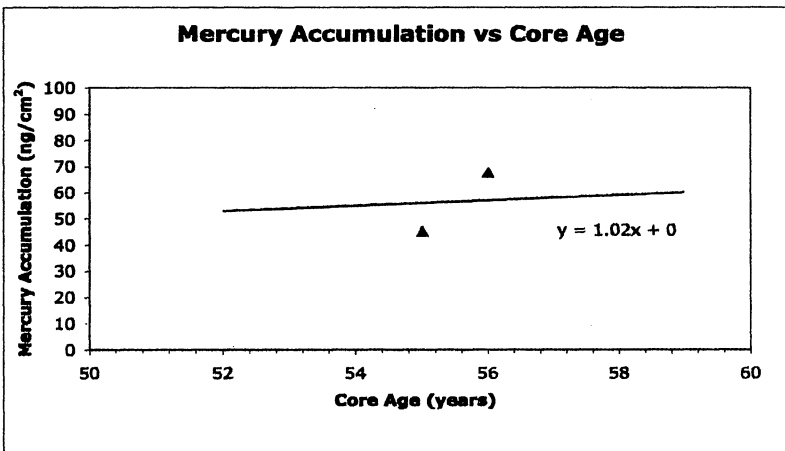


Figure 14b. Mercury accumulation (ng/cm<sup>2</sup>) in two Barrow area soil cores <100 years in age.

### Mercury Flux Calculations

It is assumed that mercury is supplied to Alaskan tundra soils solely by atmospheric deposition in a comparable manner to ombrotrophic bogs. It is also assumed that mercury is complexed by organic matter and is retained in the soil profile, as demonstrated by Drexel et al. (2002). If these assumptions are valid and a specified depth of soil has a known age the flux of mercury ( $\mu\text{g Hg m}^{-2} \text{yr}^{-1}$ ) from the atmosphere to tundra soils can be calculated.

The following calculations are used to estimate the flux of mercury to the tundra:

1.  $\text{organic layer thickness (m)} / \text{age (yr)} = \text{organic matter accumulation rate (m yr}^{-1}\text{)}$
2.  $\text{organic matter accumulation rate (m yr}^{-1}\text{)} * \text{total mercury (}\mu\text{g Hg m}^{-3}\text{)} = \text{mercury flux (}\mu\text{g Hg m}^{-2} \text{yr}^{-1}\text{)}$

Core	Organic Layer Thickness (cm)	Age of Oldest Organic Material (yr)	Organic Matter Accumulation Rate (cm yr <sup>-1</sup> )	Total Hg Content (ng cm <sup>-3</sup> )	Hg Flux (µg m <sup>-2</sup> yr <sup>-1</sup> )	Total Accumulated Hg (µg m <sup>-2</sup> )	Time Span	Adjusted Hg Flux (µg m <sup>-2</sup> yr <sup>-1</sup> )
B1	22	3700	0.006	60.4	3.59	1.33E+04	3700-2260	3.18
B1	22	3700	0.006	60.4	3.59	1.33E+04	3700-590	1.81
B2	35	2260	0.015	26.5	4.10	8.72E+03	2260-590	0.63
B3	27	3940	0.007	36.8	2.52	9.71E+03	3940-2260	0.59
B3	27	3940	0.007	36.8	2.52	9.71E+03	3940-590	0.61
B4	8	590	0.014	97.2	13.2	7.67E+03	590-55	13.3
B5	4	55	0.073	11.3	8.22	4.52E+02	55-0	8.22
B6	8	56	0.143	8.61	12.3	6.78E+02	56-0	12.3
Modern Avg.	-	-	-	-	-	5.65E+02	55-0	10.3
A1	20	1430	0.014	34.9	4.87	6.93E+03	1430-590	6.57
A2	8	590	0.014	18.8	2.39	1.41E+03	590-0	2.39
F2	7	55	0.127	16.7	19.8	1.09E+03	55-0	19.8

**Table 9. Mercury flux calculation results**

Overall the rate of organic matter accumulation declines with increasing core age. Within the mercury flux calculation, declining organic matter accumulation compensates for organic matter decomposition and the resulting soil compaction. Organic matter accumulation rates shown in table 9 in age are similar in magnitude to those reported by Hinkel et al. (2003) for Barrow area DTLB ranging from 0.009 to 0.047 cm yr<sup>-1</sup> except for the organic matter accumulation rate seen in core B6 which is nearly 3 times that of the cores studied by Hinkel et al. (2003). Core B6 comes from a young basin that might contain more rapidly growing vegetation than seen in Hinkel et al.'s basins.

Table 9 details mercury flux calculation results for the Barrow, Atkasuk, and Fairbanks area cores. The calculated fluxes represent the average net mercury load per year to each sampling location over the elapsed time each area accumulated organic material. Over the 3700 year time period in which the basin where core B1 was taken accumulated organic material it received 3.59 µg Hg m<sup>-2</sup> yr<sup>-1</sup>. Over the 2260 year time period in which the basin where core B2 was taken accumulated organic material it received 4.10 µg Hg m<sup>-2</sup> yr<sup>-1</sup>. Over the 3940 year time period in which the basin where core B3 was taken accumulated organic material it received 2.52 µg Hg m<sup>-2</sup> yr<sup>-1</sup>. Over the 590 year time period the basin in which where core B4 was taken accumulated organic material it received 13.2 µg Hg m<sup>-2</sup> yr<sup>-1</sup>. Over the 55 year time period in which the basin where B5 was taken accumulated organic material it received 8.22 µg Hg m<sup>-2</sup> yr<sup>-1</sup>. Over the 56 year time period in which the basin where B6 was taken accumulated organic material it received 12.3 µg Hg m<sup>-2</sup> yr<sup>-1</sup>. The modern mercury flux calculated as the average of the flux

recorded in cores B5 and B6 is  $10.3 \mu\text{g Hg m}^{-2} \text{ yr}^{-1}$  and is very similar to the flux estimated using the slope of the line in figure 14b.

According to Brown et al. (1980) a portion of the DTLB where core B6 was taken was manipulated in the 1970s during experiments designed to investigate the effects of human impacts on the tundra landscape. Manipulations included draining a thaw lake, heating soils, spilling oil, and causing physical disruptions with heavy machinery. Core B6 was taken well away from the site of the disturbances and within a site used for ecological research in the 1970s and 1980s. The possibility of contamination within core B6 resulting from the disturbance experiments is likely small. However, contamination stemming from either the manipulations themselves or from human activity surrounding them may in part have resulted in the higher mercury flux calculated for core B6 than was calculated for core B5.

As for the Atqasuk area soil cores, the basin from which core A1 was taken accumulated  $4.87 \mu\text{g Hg m}^{-2} \text{ yr}^{-1}$  since it began to accumulate organic matter 1430 years ago. The basin from which core A2 was taken accumulated  $2.39 \mu\text{g Hg m}^{-2} \text{ yr}^{-1}$  since it began to accumulate organic matter 590 years ago.

Additionally, while organic matter accumulation and mercury deposition processes are likely different from the tundra locations, the thermokarst area from which core F2 was taken has accumulated mercury at an approximate rate of  $19.8 \mu\text{g Hg m}^{-2} \text{ yr}^{-1}$  over the past 55 years. However, this result must be viewed as a rough estimate as the organic matter from which the radiocarbon age was derived was not cleanly picked from a sample, but was sent away for dating as a portion of a homogenized subsample. As a result, young carbon, possibly in the form of roots, may have been mixed in with older organic matter. Young carbon may have skewed the age of this core toward the modern. At this time, little else is known beyond the fact that cores F1 and F2 contain organic-rich layers near the surface and exhibit mercury concentration profiles possessing a different shape than are seen in Arctic tundra soils.

To evaluate changing mercury loading through time an adjusted mercury flux was calculated. The total mercury accumulated in the organic layer of a core ( $\mu\text{g Hg m}^{-2}$ ) was subtracted from the total mercury accumulated in an older core. The difference in accumulated mercury is divided by the time spanned in years between the age of the older basin and the younger basin. The result is the mercury flux for the time the older basin began to accumulate organic matter until the next younger basin began to accumulate organic matter. For example, core B3 accumulated  $9.71\text{E}+03 \mu\text{g Hg m}^{-2}$  and core B4 accumulated  $7.67\text{E}+03 \mu\text{g Hg m}^{-2}$  over 3940 and 590 years respectively. Therefore from 3940 to 590 years before present, a span of 3350 years,  $2.04\text{E}+03 \mu\text{g Hg m}^{-2}$  accumulated in core B3 requiring an average mercury

flux of  $0.61 \mu\text{g Hg m}^{-2} \text{yr}^{-1}$ . The results of the adjusted mercury flux calculations are expressed in table 9 and figure 15 and indicate an increasing flux of mercury to the Arctic tundra near Barrow, Alaska over time.

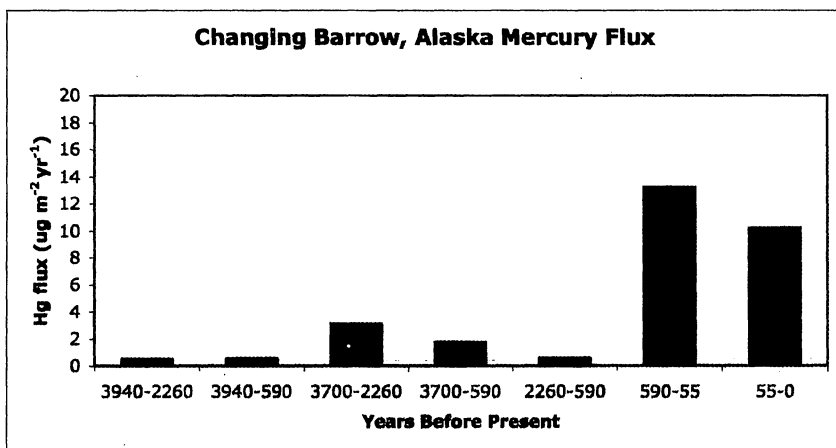


**Figure 15.** Adjusted mercury flux values derived from soil cores taken near Barrow, Alaska at various periods of time before present. The considerable difference in mercury flux values between the time periods greater than 590 years before present and those having taken place in modern times indicates increased mercury deposition in the Alaskan Arctic relative to background rates.

The adjusted mercury fluxes derived from Barrow area soil cores B1, B3, and B4 for the periods of time 3940-590 and 3700-590 years before present are  $0.61$  and  $1.81 \mu\text{g Hg m}^{-2} \text{yr}^{-1}$  respectively. Because they are the longest periods of time recorded in the DTLB profiles and they predate the industrial revolution these values can be considered the range of ‘natural’ background mercury fluxes for Arctic Alaska. As such, increases in mercury accumulation over this background range have occurred over time. The period from 590 to 55 years before present as recorded near Barrow shows a 7 to 22 fold increase in mercury flux over background levels while the flux of mercury as recorded near Barrow from 55 years before present to present day shows a 6 to 17 fold increase. The period from 590-0 years before present as recorded near Atqasuk shows a 1 to 4 fold increase in mercury flux over the background range recorded near Barrow. The Atqasuk area seemingly has not seen as dramatic an increase in mercury deposition as has taken place near Barrow potentially due to the coastal nature of MDE and Atqasuk’s inland location, but uncertainty exists as to whether this is caused by a laboratory artifact or because less mercury is deposited in the Atqasuk area that is deposited near Barrow.

The magnitude of increases in mercury flux reported here are of a similar magnitude to those reported elsewhere in the Arctic. Alaskan Arctic lake sediments indicate a 3-fold increase over the past 200 years

while blanket bog peat deposits in the Faroe Islands display a more dramatic 19-fold rise (Fitzgerald et al., 2005; Shotyk et al., 2005).

The adjusted mercury fluxes for the periods of time of 3940-2260 ( $0.59 \mu\text{g Hg m}^{-2} \text{ yr}^{-1}$ ), 3940-590 ( $0.61 \mu\text{g Hg m}^{-2} \text{ yr}^{-1}$ ), 3700-590 ( $1.81 \mu\text{g Hg m}^{-2} \text{ yr}^{-1}$ ), and 2260-590 ( $0.63 \mu\text{g Hg m}^{-2} \text{ yr}^{-1}$ ) years before present calculated here are in agreement with other reported background fluxes as recorded in peat archives. In the Arctic, Givelet et al. (2004a) report a background flux of  $\sim 1 \mu\text{g Hg m}^{-2} \text{ yr}^{-1}$  on Bathurst Island in similar terrain to the tundra landscape near Barrow and Shotyk et al. (2005) report a background flux of  $1.27 \mu\text{g Hg m}^{-2} \text{ yr}^{-1}$  on the Faroe Islands. Other northern latitude mercury studies investigating peat archives in Norway, Switzerland, Sweden and Greenland also show low pre-industrial background mercury fluxes ranging from  $0.3$  to  $1.6 \mu\text{g Hg m}^{-2} \text{ yr}^{-1}$  (Steinnes et al., 2005; Roos-Barraclough and Shotyk, 2003; Roos-Barraclough et al., 2002a; Bindler, 2003; Shotyk et al., 2003). In North America, Givelet et al. (2003) report a background flux as recorded in Ontario, Canada peat of  $1.4 \mu\text{g Hg m}^{-2} \text{ yr}^{-1}$ .

Site	Years BP	Sampling Location	Author	Hg Flux ( $\mu\text{g Hg m}^{-2} \text{ yr}^{-1}$ )
Bathurst Island (background)	5900-800	peat hummocks	Givelet et al., 2004a	0.5 to 1.5
Faroe Islands (natural)	3525-620	blanket bog	Shotyk et al., 2005	$1.27 \pm 0.38$
Faroe Islands (max)				34
Faroe Islands (1998)				16
Norway (pre-ind)	2000-1000	ombrotrophic bogs	Steinnes et al., 2005	0.3 to 0.9
Norway (post-ind)	100-0			2.1 to 11.1
Switzerland, Jura Mtns (background)	>663	ombrotrophic bogs	Roos-Barraclough and Shotyk, 2003	$1.0 \pm 0.3$ to $1.6 \pm 0.4$
Switzerland, Jura Mtns (natural)		ombrotrophic bogs	Roos-Barraclough et al., 2002a	0.3 to 8.0
Switzerland, Jura Mtns (max, ~1900)				107.6
Switzerland, Jura Mtns (1970's)				78.8
Southern Sweden	4000-500	ombrotrophic bogs	Bindler, 2003	0.5 to 1
Southern Sweden	1942-1991			23 to 25
Greenland (min)	1031-1456	minerotrophic fen and ombrotrophic bog	Shotyk et al., 2003	0.5
Greenland (max, 1953)				164
Greenland (1995)				14
Ontario (background)	7706-536	ombrotrophic bogs	Givelet et al., 2003	$1.4 \pm 1.0$
Ontario, urban area (max, ~1958)				141
Ontario, agricultural area (max, ~1958)				89
Ontario, forested area (max, ~1958)				54

**Table 10.** Published mercury flux results for the Arctic and cold regions around the northern hemisphere.



The adjusted mercury flux for the period of 3700-2260 years before present ( $3.18 \mu\text{g Hg m}^{-2} \text{yr}^{-1}$ ) is curiously elevated in comparison with published background mercury fluxes from cold regions in the northern hemisphere. As was discussed previously, core B1, upon which this adjusted mercury flux is based, has potentially been contaminated by an intrusion of lacustrine sediments into its upper 10 cm. As seen in figure 8, core B1 contains elevated density measurements over those expected from pure organic-rich sediments. The elevated densities may have led to overestimated total mercury content which is the product of density and mercury concentration. Overestimated mercury content could have caused the overestimated mercury flux values calculated for the period of time of 3700-2260 years before present.

The temporal resolution of the adjusted mercury fluxes could be better given additional known ages within the peat profiles. Of particular interest is the time period of 590 to 55 years before present recorded in core B4. This period of time encompasses the industrial revolution and dawn of the anthropocene (ca. 1800), a time of increasing anthropogenic mercury emissions due to the widespread combustion of coal. It would be insightful to be able to divide the 590 to 55 years before present time span into periods of 590-205 and 205-55 years before present. An estimated mercury flux for this period of time can be calculated if it is assumed that from 590 to 205 years before present the flux was  $4.10 \mu\text{g Hg m}^{-2} \text{yr}^{-1}$ . This number is taken from the average flux calculated for ‘ancient’ core B2 and represents the time when industrial activity had yet to commence and the mercury flux to the Arctic was likely low. It follows that if the flux from 590-55 years before present was  $13.3 \mu\text{g Hg m}^{-2} \text{yr}^{-1}$  as reported above then the mercury flux from 205-55 years before present must be  $\sim 37 \mu\text{g Hg m}^{-2} \text{yr}^{-1}$ . See equations 3 and 4 below.

$$\text{average flux} = (\text{flux}_1 * \text{years in period 1} + \text{flux}_2 * \text{years in period 2}) / \text{total years} \quad \text{eqtn. 3}$$

$$\text{flux}_2 = \text{average flux} * \text{total years} - \text{flux}_1 * \text{years in period 1} / \text{years in period 2} \quad \text{eqtn. 4}$$

Despite the considerable uncertainty in the above estimation, it is likely that a dramatic increase in mercury flux over the latter part of the 590 to 55 years before present time span took place to increase the flux during this time to  $13.3 \mu\text{g Hg m}^{-2} \text{yr}^{-1}$  from the  $4.10 \mu\text{g Hg m}^{-2} \text{yr}^{-1}$  calculated for the period of 2260 to 0 years before present.

One potential limiting factor in the adjusted mercury flux calculation is that if the ‘old’ and ‘ancient’ DTLB experience a slowed mercury accumulation rate as the accumulation of organic matter slows. If the ‘ancient’ basins accumulate less mercury over time then subtracting the mercury from the cores from basins of ‘young’ age would yield an underestimate of total accumulated mercury and adjusted mercury

flux. However, in examining mercury concentration profiles in figure 10a it appears more likely that the basins have continued to accumulate mercury resulting in the extraordinary mercury concentrations atop the older tundra soil cores.

#### *The Merits of Using DTLB to Estimate Hg Fluxes*

In other studies utilizing peat cores to establish historical mercury fluxes ages and mercury content are determined for individual core layers. A mercury flux is calculated for each point in the core's depth profile. Since it is possible that minor disturbances may have taken place within the organic layer of the tundra soil cores due to soil mixing or due to supplementary deposition of mercury in desiccation cracks the likelihood of producing viable results using the established method is small. It is reasonable to expect that the method proposed here of calculating mercury fluxes based on subtracting the accumulated mercury of a core of known age from that of another core of known age will meet with more success in the dynamic tundra environment than traditional methods used in the study of peat bogs. The potential complications of ice-induced disturbances are lessened when mercury accumulation is considered across the entire organic layer thickness. No one disturbed layer will have an overbearing impact on the flux calculations. For example, if, as previously discussed, the organic layer of core B1 contains an intrusion of lacustrine sediment the impact of that disturbance as far as an artificial increase in bulk density and/or an artificial decrease in mercury concentration would have but a minor effect on the core's integrated total mercury content.

#### *Mercury Depletion Events*

Lindberg et al. (2002) suggest that due to MDE the depositional flux of mercury in Barrow, Alaska from January to May is  $\sim 55 \mu\text{g Hg m}^{-2}$ . The modern mercury flux recorded in the Arctic tundra soils considered here is 5 times less than this; the difference between the MDE flux and the modern annual flux is  $45 \mu\text{g Hg m}^{-2}$ . This suggests that either MDE are a new phenomenon too recent in origin to have been well recorded in the sedimentary record or that mercury fluxes derived from organic-rich tundra soils do not equate with atmospheric depositional fluxes. Regarding the accumulation rate of mercury in tundra soils versus rates of atmospheric mercury deposition during MDE, the flux recorded in the soils may be smaller in magnitude than reported values for the atmospheric deposition flux. Near Barrow, mercury loading happens largely in the spring months due to MDE when snowpack exists across the landscape (Lindberg et al., 2002). After deposition to the snowpack, much of the deposited mercury is lost to the atmosphere from the snow surface as mercury is photoreduced from ionic mercury ( $\text{Hg}^{2+}$ ) to gaseous elemental

mercury (St. Louis et al., 2005). It has been reported that total snowpack mercury levels decline by up to 92% within two days of an MDE (Poulain et al., 2004). Later, during spring snowmelt, more mercury deposited during MDE becomes unavailable for accumulation in the soil profile. The tundra snowpack melts rapidly because of the expeditiously increasing amount of solar energy reaching the landscape after polar sunrise. It is during snowmelt that Arctic rivers contain their maximum dissolved organic content (Rember and Trefry, 2004). As reported in lower latitude locations and in the Arctic mercury is flushed into drainages bound to dissolved organic carbon during these spring flood events (Shanley, et al., 2002; Losetto et al., 2004). Only a portion then of springtime deposited mercury sorbs to organic matter at the top of the soil profile and accumulates there after losses of mercury during photoreduction and snowmelt runoff. Hence, while mercury deposition to the tundra near Barrow may be extreme due to MDE, it is probable that soil profiles presented here reveal a dampened depositional record. In this case MDE may have begun sometime between 590 and 55 years before present when mercury fluxes became elevated over background levels as seen in figure 15. Also supporting the notion of recent onset of MDE is the agreement of Barrow area background mercury fluxes calculated in this work ( $0.61$  to  $1.81 \mu\text{g Hg m}^{-2} \text{yr}^{-1}$ ) with the published background values seen table 10. It is likely that if areas known not to experience MDE, such as the Jura Mountains of Switzerland (background flux:  $1.0$  to  $1.6 \mu\text{g Hg m}^{-2} \text{yr}^{-1}$ ), have similar background mercury fluxes to those seen in Arctic Alaska that similar non-MDE mercury deposition processes would have been at work in both places.

## Conclusions

In conclusion, with respect to how mercury concentrations change in soil cores with depth, mercury concentrations in Alaskan Arctic tundra soil profiles are at a maximum near the surface and decrease through the organic layer. This pattern suggests increasing mercury deposition through time. With respect to corroboration of reports of increasing mercury deposition across the Arctic, this work illustrates that the modern flux of mercury to the Arctic tundra of Alaska is at least 6 times increased over background levels. Also, the 'natural' background mercury flux derived from the tundra soil cores is similar to background fluxes reported elsewhere in the Arctic and throughout the northern hemisphere. As to insight on the spatial extent of MDE, it is likely that MDE play a key role in mercury deposition to tundra soils along the Alaskan Arctic coastline and that MDE have played some role in increased modern inland mercury deposition. This is seen in the elevated mercury flux derived from Atkasuk area soil cores with respect to background fluxes as well as in the high mercury concentrations near the surface in Atkasuk soil cores. MDE may be regional in extent rather than a purely a coastal phenomenon, however the effects of MDE in terms of increased mercury flux are more certain in the coastal Barrow area than farther inland

at Atqasuk. As for MDE onset, it is likely that MDE are recent in origin, but are not well recorded at this point in Alaskan Arctic tundra soils. Finally, tundra soils may play only a small role in retaining mercury deposited in MDE when compared to revolitization of mercury from the snowpack and to runoff during the spring thaw.

## **Appendix A: Field Description of Soil Cores with Depth (cm)**

### **B1**

0-1	very dark brown peat
1-4.5	dark brown peat
4.5-12	light brown silt rich sediments
12-17	medium brown peaty sediments
17-23	darker brown peaty sediments
23-25	peat (dark brown sediments)

### **B2**

0-1.5	roots and green moss
1.5-6.5	light to medium brown roots/peat
6.5-9	dark to reddish brown peaty silt
9-12	dark brown peat
12-23	dark brown silty peat
23-26	black/dark brown peaty silt

### **B3**

0-4	oi, uncompressed organic material
4-16	oe, partially decomposed organic material (interbedded silt and loam)
16-28	o, dark sediments containing decomposing organic material (tussocky)
28-31	bottom of the active layer
31-45	frozen silt/loam

### **B4**

0-1	green moss and light brown roots
1-3	dark brown intermixed moss, roots, peat
3-8	dark brown peat with roots
8-25	medium brown peaty silt

### **B5**

0-2	grass and roots
2-4	roots and sediments
4-26	medium brown silt-rich sediments

### **B6**

0-4	tall grass and mossy plant material
4-8	dark brown, plentiful roots and decomposed plant material
8-11	almost pure root material
11-15	root material mixes with dark brown peat
15-27	gray silty sediments mixed with brown peat

### **A1**

0-1	moss and grass
1-7	orange decaying peat/sphagnum moss
7-12	brown peat
12-22	black to brown peat

A2

0-2 green living material (mossy)  
2-6 orange slightly-decomposed material  
6-8 sand mixed with decomposed organic material  
8-12 dark brown silt with organic material  
12-18 medium brown peaty silt  
18-26 slightly lighter brown peat with some sand and reddish silty layers (18-19 cm)

F1

0-2 green/yellow moss with leafy green plant material  
2-3 mottled brown roots, peat and yellow moss  
3-8 dark brown roots, peat  
8-10 dark brown peaty silt  
10-28 light brown silt  
28-39 darker brown peaty silt

F2

0-1 green moss  
1-6 light to dark brown peaty material mixed with vegetation and roots  
6-8 dark brown peat  
8-18 dark brown peaty silt  
18-44 medium brown silt

## **Appendix B: Analysis of Solid Samples Using the Nippon Instruments MA-2000 Mercury Analyzer:**

### **Preparation of powders:**

- Bake Nippon Instruments M & B powders (M: 64% Na<sub>2</sub>CO<sub>3</sub>, 36% Ca(OH)<sub>2</sub>; B: Al<sub>2</sub>O<sub>3</sub>) in large ceramic crucibles inside a muffle furnace @ 750° C for 3 hours to remove trace mercury contamination.
  - Before using powders on subsequent days after the three-hour bake, bake powders for an additional 1 hr @ 750° C.
  - Store baked M & B powders in the desiccation box and not in the drying oven to reduce possible spread of M & B powder dust.
- Allow powders to cool before use.
- Wash stainless scoop used in ladling the powders before each use and after each subsequent use with 2x DI water.
- If needed, order replacement powders at the end of a run so they are immediately available for the next run.

### **Preparation and cleaning of sample boats:**

- Bake dry empty ceramic boats in a muffle furnace @ 750° C for 1 hr to remove trace mercury contamination.
- To clean the boats after they have been filled and used to run a sample or standard:
  - Transfer the used boats from the MA-2000 in a closed plastic container to the hood where boats are filled and place the full used boats into a zip-lock bag. Seal the zip-lock bag.
  - Transport the full used boats in their zip-lock bag upstairs to the 'peat-cutting room' (the 5<sup>th</sup> floor space we share with Dr. Ben van der Pluijm's group and others).
  - Inside the filtered dust-control box gently scrape the powders/sample residues from the boats into the zip-lock bag in which they were carried upstairs.
  - Discard the zip-lock bag filled with used powders in the 5<sup>th</sup> floor trash.
  - Submerge the scraped boats into a water-filled plastic container.
  - Bring the submerged boats back down to room 4006 and rinse them with hot tap water while scrubbing them gently with a soft brush to remove any residue.
  - Rinse the boats in 2x DI water.
  - Place the boats in a room temperature HCl bath (5-10% acid). Soak for at least ½ hour.
  - Remove the boats from the acid bath and rinse them thoroughly with 2x water.
  - Place boats in the drying oven at ~70 °C until dry.
  - Bake boats in muffle furnace @ 750 °C for 1 hr.
  - Store clean boats in the drying oven at ~70 °C.

### **Preparation of standard solutions:**

- Clean glassware that will hold standards: rinse thoroughly with 2x water, fill 2/3 with 1% BrCl, soak ~1 day, invert, and soak another ~1 day, rinse ≥5 times with 2x water, dry in a laminar flow hood.
- Using purged reagents, make 0.001% L-cysteine solution as directed by the MA-2000 manual: add 10 mg of L-cysteine solid to a 1000 mL flask, add 2 mL purged reagent grade nitric acid, and fill to 1000 mL with 2x DI water.

- Dilute the 1001 mg/L Hg (HgCl<sub>2</sub>) standard (1001 ppm) 100 times in 0.001% L-cysteine solution (1g/100g) to make 10.01 ppm standard. Dilute the 10.01 ppm an additional 100 times to make 100.1 ppb standard.
- On the first day of the run and after each 2-3 days thereafter make a ~20 ppb Hg solution by diluting the 100.1 ppb standard 1 to 5 in 0.001% L-cysteine solution in a small, clean glass bottle (with teflon-lined cap).
- Follow the directions in the MA-2000 manual for prepping boats for liquid samples/standards: add a layer of B powder, followed by the liquid standard, followed by another layer of B powder, capped by a layer of M powder. Powders should have been previously baked as described above.
- Prepare the calibration standards by pipetting 0.05, 0.10, 0.25, 0.50, 0.75, and 1.00 grams of the 20 ppb solution (1, 2, 5, 10, 15, 20 nanograms of Hg) into prepared boats.
- Prepare check standards by pipetting 0.50 grams of 20 ppb solution (10 ng Hg) into prepared boats.

Preparing the MA-2000 for use in mercury analysis of peat/soil samples:

- Wait for the MA-2000's furnaces to cool to room temperature before conducting any maintenance or repairs. The combustion tube is fragile and easily broken when hot.
- In ~5% HNO<sub>3</sub> soak the glass bulb that attaches to the furnace tube, the glass bubblers, the teflon connectors, and the 3-pronged glass tubing. Rinse each well with 2x DI water. Dry each in a laminar flow hood. Reassemble the MA-2000. Run 'leak check' in the 'Run' menu: 'Mainte' after the MA-2000 is reassembled. Gently insert the rubber stopper into the furnace tube before the leak check and be sure to turn off the pump before removing the stopper. Gently allow air to return to the system. Rapid re-pressurization can cause catastrophic flash heating of water inside the furnace tube resulting in a shattered tube.
- In the 'System' menu: 'Setup': check that attached equipment reads 'BC'
- In 'Run' menu: 'Mode': Set to run on 'Mode 2' and set measurement mode to 'Low'
- In 'Table' menu: 'Table Condition':
  - Set method to 'heating'
  - Set sample to 'solid'
  - Set STD to 'amount'
  - Set Standard to 'ng'
  - Set amount to 'mg'
  - Set mercury to 'ng'
  - Set concentration to 'ppb'
  - Set PEAK/INTE to 'peak'
  - Set Calibration Curve to 'y=ax+Blank'
- In Run menu: Mainte: check and record signal voltage 'Sig(v)' and reference voltage 'Ref(v).' These should both be ~4.000. Large differences between the signal and reference voltages could mean a problem with the MA-2000. If the signal voltage is depressed, depressed absorbances and hence lower than actual mercury concentrations could result.
- Change the buffer solution (pH 7 phosphate buffer solution is used during solids analyses) every 2-3 days of running. The glass bubbler containing the buffer solution tends to increase over time due to small additions of moisture from the samples and from the air in the instrument room. The bubbler should be drained and the buffer solution replaced before the level of the solution reaches half-way up the bubbler.
- Check for system leaks every 2-3 days or when the buffer solution is changed. Again, use extreme caution not to allow liquids to shoot up into the combustion tube. A leak check where the flow of air as gauged at the flow meter does not lessen likely indicates a broken combustion tube. A leak check where the flow lessens but where the ball in the flow meter does not come to complete rest likely indicates a leak due to a faulty connection within the MA-2000.



### Running solid sample analyses on the MA-2000:

- Run  $\geq 7$  empty boats and examine the results before running calibration standards to ensure that the boats are clean, that the system is purged of mercury, and that the MA-2000 blank's absorbance is  $< 0.005$ .
- Prepare the calibration standards as described above.
- After running the calibration standards check that the 20 ng standard's absorbance is  $\sim 1.0$ . Divide the abs by the actual ng of Hg pipetted into the boat. The abs/ng Hg ratio on a daily basis should be around 0.056. If the abs for the 20 ng standard is less than 1.0 then either the standard has lost mercury and is bad or the MA-2000 has a depressed ability to detect mercury and should be cleaned. Recheck the signal and reference voltages.
- Prepare boats as directed by the MA-2000 manual: for solid samples, add a layer of M powder, the sample/standard, a second layer of M powder, a layer of B powder, and a final layer of M powder. Add the powders to the boats inside a fume hood to limit dust transport throughout the lab.
- Tare each boat after the addition of the first layer of M powder then record the mass of sample added to each.
- Add approximately 100 mg of sample material to each sample boat and attempt to distribute the material over the entire length of the boat. Adjust this amount as necessary to add no more than 20 ng of Hg to any boat as 20 ng of Hg is the limit of the MA-2000's 'Low' mode.
- Use a stainless steel spatula to add powdered solid material to the boats. Rinse the spatula with 2x DI water between samples. Make ample use of the anti-static gun to limit flyaway of sample powder.
- Run this pattern: one blank (powders only), one check standard ( $\sim 10$  ng Hg), a purge, 6 samples with a purge between each sample, one replicate sample, a purge, a second check standard, a purge, and a second blank.
- Purges are absolutely necessary when running organic-rich sample materials. It is our hypothesis that for an unknown reason combusting organic-rich materials causes the mercury signal to be depressed possibly because the gold trap is not able to capture all of the mercury released from each sample. Running purges between samples seems to clean the gold trap and restore it to its full ability to trap mercury. When purges are not run between samples resulting sample Hg concentrations are up to 100% lower than when purges are run.
- To limit dust generation, transport samples in a closed plastic container between room 4006 where the sample-pouring hood is and the MA-2000 in the instrument room.
- Every day save MA-2000 data files and transfer the data to an excel file; every day export the excel file to email.

### Cleaning up:

- Wipe down lab surfaces as soon as possible after making sample and standard boats, especially if leaving room 2006 for an extended period of time. Be sure to wipe down the bench tops, wipe down the hood, and wipe down the balance.
- Wipe down the area (bench top and floor) around the MA-2000 regularly during sample run periods.
- Swiffer the floor in room 2006 every 3-4 days.
- Discard all objects that come into contact with powders or powdered samples (gloves, kimwipes, paper towel, crew wipes, empty powder bottles, etc.) into a zip-lock bag that resides in the sample pouring fume hood. When this zip-lock is full, seal it carefully and discard it into the trash.
- Clean up spills in the instrument room of M & B powders and powdered samples immediately.

## Appendix C.

### **General Statement of $^{14}\text{C}$ Procedures at the National Ocean Sciences AMS Facility (provided by NOSAMS).**

All laboratory preparations for AMS radiocarbon analyses of submitted samples occur in the NOSAMS Sample Preparation Lab unless otherwise noted on the attached report of Final Results. Procedures appropriate to the raw material being analyzed include: acid hydrolysis (HY), combustion (OC), or stripping of  $\text{CO}_2$  gas from water (WS) samples. Carbon dioxide, whether submitted directly (GS) or generated at the NOSAMS Facility, is reacted with catalyst to form graphite. An Fe/ $\text{H}_2$  catalytic-reduction is used for all except very small samples, where a Co/ $\text{H}_2$  catalytic-reduction is used. Graphite is pressed into targets, which are analyzed on the accelerator along with standards and process blanks. Two primary standards are used during all  $^{14}\text{C}$  measurements: NBS Oxalic Acid I (NIST-SRM-4990) and Oxalic Acid II (NIST-SRM-4990C). The  $^{14}\text{C}$  activity ratio of Oxalic Acid II ( $\delta^{13}\text{C} = -17.3$  per mil) to Oxalic Acid I ( $\delta^{13}\text{C} = -19.0$  per mil) is taken to be 1.293. Every group of samples processed includes an appropriate blank, which is analyzed concurrently with the group. Process blank materials include IAEA C-1 Carrara marble for inorganic carbon and gas samples; a Johnson-Mathey 99.9999% graphite powder for organic carbon samples; and a commercial tank of  $^{14}\text{C}$ - free  $\text{CO}_2$  for seawater samples.

Fraction Modern ( $F_m$ ) is a measurement of the deviation of the  $^{14}\text{C}/\text{C}$  ratio of a sample from "modern." Modern is defined as 95% of the radiocarbon concentration (in AD 1950) of NBS Oxalic Acid I normalized to  $\delta^{13}\text{C}_{\text{VPDB}} = -19$  per mil (Olsson, 1970). AMS results are calculated using the internationally accepted modern value of  $1.176 \pm 0.010 \times 10^{-12}$  (Karlen, *et. al.*, 1968) and a final  $^{13}\text{C}$  correction is made to normalize the sample  $F_m$  to a  $\delta^{13}\text{C}_{\text{VPDB}}$  value of -25 per mil.

Stable isotope measurements of sample  $\delta^{13}\text{C}$  used to correct  $F_m$  values are typically made at the NOSAMS Facility by analyzing sub-samples of the  $\text{CO}_2$  gas generated during graphite production with either a VG PRISM or VG OPTIMA mass spectrometer. However, some carbonate samples are reacted and measured directly with the VG PRISM ISOCARB. The  $\delta^{13}\text{C}$  value used to calculate the  $F_m$  of a sample is specified in the report of Final Results.

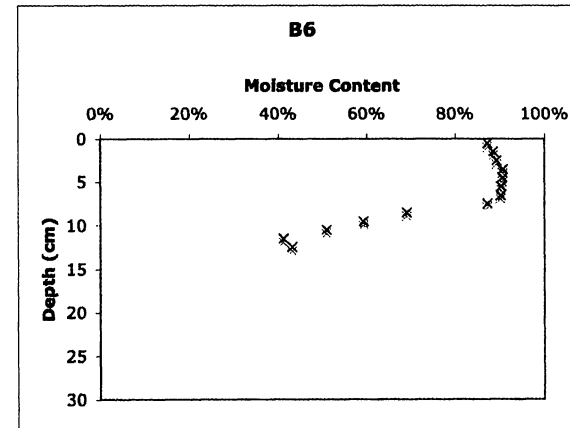
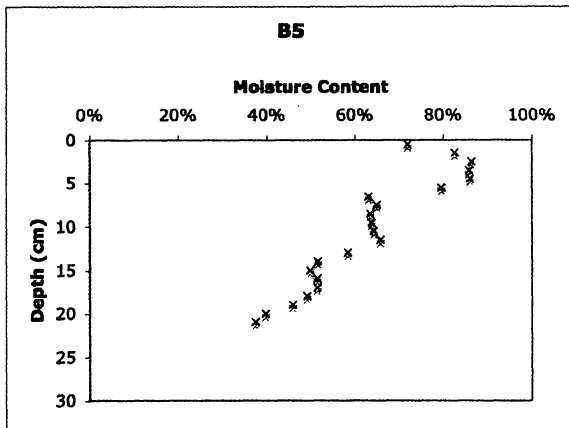
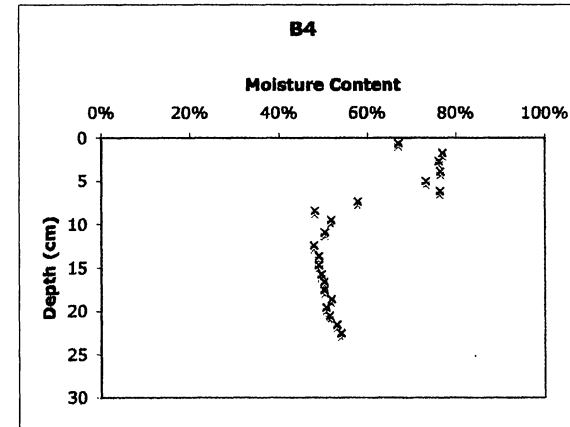
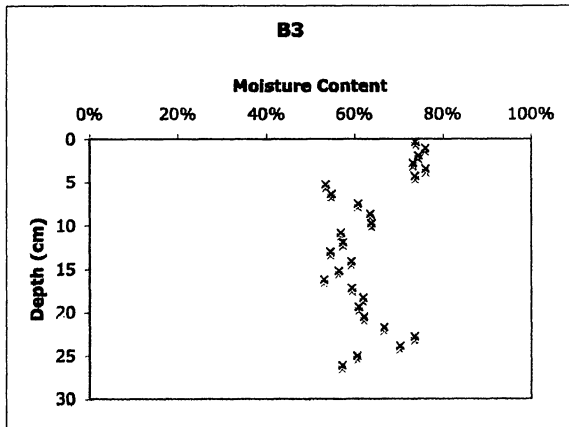
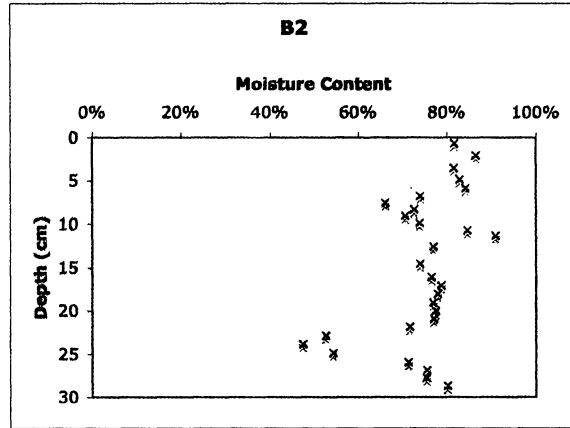
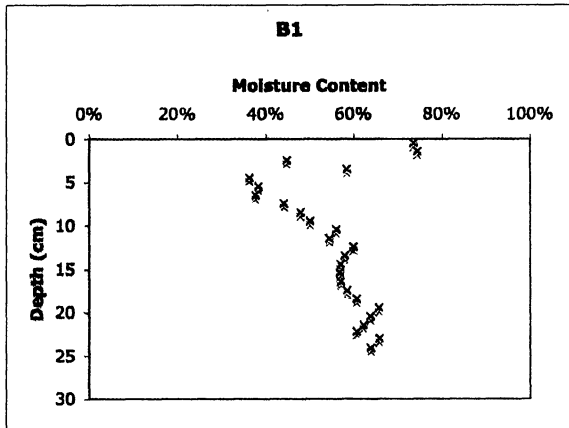
Reporting of ages and/or activities follows the convention outlined by Stuiver and Polach (1977) and Stuiver (1980). Radiocarbon ages are calculated using 5568 (yrs) as the half-life of radiocarbon and are reported without reservoir corrections or calibration to calendar years. For all sea water samples, where collection date is known, a  $\Delta^{14}\text{C}$  activity which has been corrected to 1950 5/27/99 values is also reported. For other samples where  $\Delta^{14}\text{C}$  is reported, we assume the collection and measurement date are the same and leave it to the submitter to make further age corrections. Atoms of  $^{14}\text{C}$  contained in a sample are directly counted using the AMS method of radiocarbon analysis, therefore, internal statistical errors are calculated using the number of counts measured from each target. An external error is calculated from the reproducibility of individual analyses for a given target. The error reported is the larger of the internal or external errors.

When reporting AMS results of samples run at the NOSAMS facility, accession numbers (e.g. OS-####'s) are required to be listed together with the results. To avoid confusion, we suggest tabulating OS-numbers and associated radiocarbon ages as they appear on the attached Final Report in addition to any subsequent corrections that may need to be made to the ages. We ask that published results acknowledge support from NSF by including the NSF Cooperative Agreement number, OCE-9807266. The NOSAMS facility would appreciate receiving reprints or preprints of papers referencing AMS analyses made at the NOSAMS facility. Any sample material not consumed during sample preparation or AMS radiocarbon analysis is archived for two years at the NOSAMS Facility unless other arrangements are made by the submitter.

**NOSAMS REFERENCES:**

- Karlen, I., Olsson, I.U., Kallburg, P. and Kilici, S., 1968. Absolute determination of the activity of two  $^{14}\text{C}$  dating standards. *Arkiv Geofysik*, 4:465-471.
- Olsson, I.U., 1970. The use of Oxalic acid as a Standard. *In* I.U. Olsson, ed., *Radiocarbon Variations and Absolute Chronology*, Nobel Symposium, 12th Proc., John Wiley & Sons, New York, p. 17.
- Stuiver, M. and Polach, H.A., 1977. Discussion: Reporting of  $^{14}\text{C}$  data. *Radiocarbon*, 19:355-363.
- Stuiver, M., 1980. Workshop on  $^{14}\text{C}$  data reporting. *Radiocarbon*, 22:964-966.

Appendix D. Moisture Content Figures



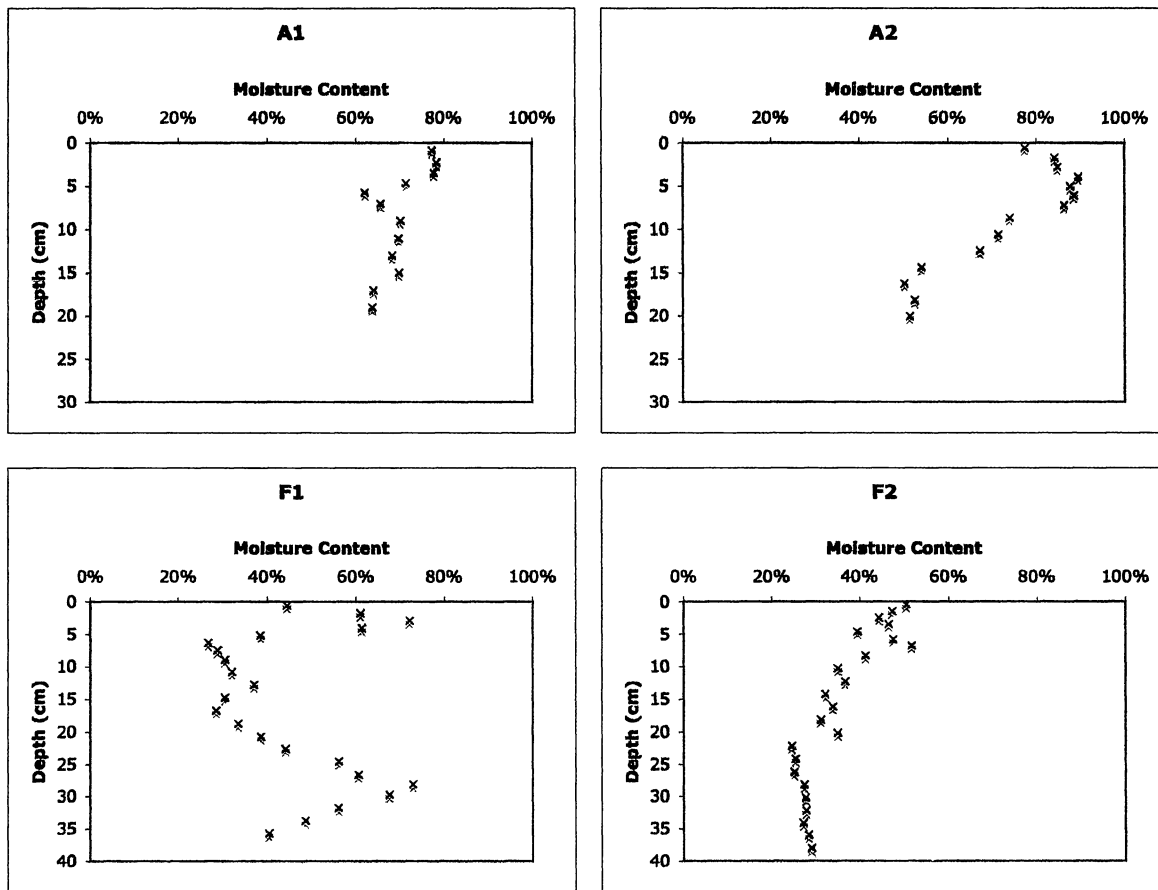


Figure 16. Alaskan soil core moisture contents.

**Appendix E. Summary of Liquid Analysis Tests With Regards to High Organic Content Samples.**

Liquid water samples collected near Barrow, Alaska during snowmelt and post-snowmelt conditions tend to be enriched in organic material. They are yellow to brown in color due to high contents of dissolved and suspended organic matter.

In preparation for previous analyses of snow samples that were clear in color and seemed to contain minimal organic material, to each sample was added concentrated bromine chloride (BrCl) to a concentration of 1% (by mass). BrCl is an oxidant and as such oxidizes mercury to its relatively stable Hg<sup>2+</sup> state. In addition to oxidizing mercury, BrCl partially oxidizes organic material and can cause the release of sorbed mercury. Samples are digested in 1% BrCl for a minimum of 24 hours before analysis using the Nippon Instruments MA-2000 mercury analyzer.

Due to the recalcitrant nature of the organic material and its abundance in the snowmelt/post-snowmelt liquid water samples, the digestion regime used on snow samples was insufficient to prepare the liquid water samples for analysis. In fact, a 5-fold increase in BrCl concentration (5%) was also insufficient. The organic matter was insufficiently broken down leading likely to incomplete release of sorbed mercury and, more dramatically, to an inability of the MA-2000 to detect mercury perhaps due to poisoning of the gold trap. As seen in table E1, after the first sample was analyzed following check standards are well below expected values. Subsequent samples show mercury concentrations below the level of the laboratory blank as denoted by a negative mercury concentration. The expected mercury concentrations for these samples are in the 10 ppt (ng/kg) range.

Sample No.	Absorbance	Hg (ppt)	Notes
CHECK STD (~10 ppt)	0.004747	8.59	15% error
442-5W6 (5%)	0.001360	2.17	
454-5W6 (5%)	0.000691	0.45	
442-5W31 (5%)	0.000726	-0.09	
Emu 3 (5%)	0.000273	-0.39	
423-5W116 (5%)	0.000633	0.33	
CHECK STD (~10 ppt)	0.002830	4.74	53% error
458-5W69 (5%)	0.001412	1.89	
442-5W39 (5%)	0.000880	0.83	
Emu 2 (5%)	0.000213	-0.51	
406-5W44 (5%)	0.000198	-0.54	
CHECK STD (~10 ppt)	0.000757	0.58	94% error

The rapidly decreasing absorbance values can be explained in a variety of ways. First, mercury could be lost from the samples prior to analysis or could be steadily lost as samples await being run in the MA-2000's sample holding tray. This notion is countered by examining the next three analyses (table E2) after those presented in table E1. After two additional runs the expected mercury concentration rebounds. This indicates that mercury is not lost pre-analysis and that another explanation must be sought. To further assure that mercury is not lost before analysis it is recommended that during pre-reduction where hydroxylamine hydrochloride ( $\text{NH}_2\text{OH}\cdot\text{HCl}$ ) is added to each sample to mitigate  $\text{BrCl}$ 's oxidative abilities only 0.020 mL of  $\text{NH}_2\text{OH}\cdot\text{HCl}$  is added to a 5 mL sample in 1%  $\text{BrCl}$ . Previously, this lab had used ~0.10 mL of  $\text{NH}_2\text{OH}\cdot\text{HCl}$ . Lessening the  $\text{NH}_2\text{OH}\cdot\text{HCl}$  added to each sample lessens the chance that  $\text{NH}_2\text{OH}\cdot\text{HCl}$  will reduce  $\text{Hg}^{2+}$  to  $\text{Hg}^0$  (g). If a 5 mL sample is in a 5%  $\text{BrCl}$  solution then it is recommended that 0.050 mL of  $\text{NH}_2\text{OH}\cdot\text{HCl}$  be used in pre-reduction.

Sample (µg)	Absorbance	Hg (ppt)
water	0.000428	-0.08
1% BrCl	0.00083	0.29
CHECK STD (~10 ppt)	0.004220	7.54

This led the idea that mercury is not quantitatively trapped because of a deleterious interaction between the gold plating in the gold trap and volatile organic compounds. Perhaps the cleansing runs seen in table E2 are gradually clearing the gold trap of contamination via combustion as the trap is heated to 650 °C in order to release trapped mercury. Perhaps the samples need additional treatment to reduce the effect the organics have on the MA-2000.

It was therefore decided that the Alaskan liquid samples would be subjugated to additional oxidative treatment in an effort to limit the organically induced interference. Three further treatments were proposed: hot nitric acid ( $\text{HNO}_3$ ) digest, hydrogen peroxide ( $\text{H}_2\text{O}_2$ ) digest, and treatment with ultraviolet (UV) radiation. An experiment involving each of these was then carried out. Confounding variables such as dirty glassware, dirty tubing/connections in the MA-2000, and bad reagents ( $\text{SnCl}_2$ ,  $\text{BrCl}$ , and  $\text{NH}_2\text{OH}\cdot\text{HCl}$ ) were carefully controlled during the experiments as glassware and the MA-2000's removable parts were thoroughly cleaned (acid-washed) and new reagents were made.

During the hot  $\text{HNO}_3$  digest experiment, purged concentrated nitric acid was added bringing the ratio of sample to acid to 2:1 by mass. Approximately 4 g of  $\text{HNO}_3$  was added to approximately 8 g of sample. The solutions were heated on a hot plate at 70 °C overnight in pre-cleaned teflon beakers. The solutions

were diluted with reagent water 50:50 before analysis. This experiment offered few positive results (table E3). Again a rapid decrease in absorbance and mercury concentration was seen after running a high organic content liquid sample. Also, the procedural check standard seems to have lost mercury, perhaps during heating, and is followed in the run by a spurious check standard mercury concentration. This method of oxidation was discarded because of these results and because of trepidation of introducing extremely acidic samples into the MA-2000.

Sample Info	Absorbance	Hg (ppt)
BW08HgU	0.000310	-0.62
CHECK STD (~20 ppt)	0.000241	-0.33
CHECK STD (~20 ppt)	0.000431	-0.33
CHECK STD (~20 ppt)	0.005896	12.86
CHECK STD (~20 ppt)	0.00741	24.99
CHECK STD (~20 ppt)	0.008320	18.72
CHECK STD (~20 ppt)	0.00927	33.12
CHECK STD (~20 ppt)	0.010917	24.99
CHECK STD (~20 ppt)	0.009014	20.39

During the H<sub>2</sub>O<sub>2</sub> digest, H<sub>2</sub>O<sub>2</sub> was added to the liquid sample to create a 1 molar H<sub>2</sub>O<sub>2</sub> solution. The solutions sat overnight in sealed pre-cleaned teflon beakers. It was noticed that upon the addition of H<sub>2</sub>O<sub>2</sub> bubbling occurred perhaps leading to loss of mercury. Table E4 shows the results of this experiment. The process blank gained a minute amount of mercury while sample mercury concentrations increased dramatically contrary to expectations. Unfortunately, check standards following H<sub>2</sub>O<sub>2</sub> digested samples show artificially elevated mercury concentrations and require several replicate checks to be run before settling again to expected levels. These curious findings lead to the abandonment of this method of oxidation.

Sample Info	Absorbance	Hg (ppt)
CHECK STD (~20 ppt)	0.008676	19.34
Process blank	0.000790	1.45
CHECK STD (~20 ppt)	0.008537	19.02
CHEM 15	0.034269	77.40
CHECK STD (~20 ppt)	0.025224	56.88
CHECK STD (~20 ppt)	0.009551	22.07
CHECK STD (~20 ppt)	0.008969	20.00
CHECK STD (~20 ppt)	0.009035	20.15
05BW08HgU	0.014749	33.12



CHECK STD (~20 ppt)	0.009997	22.34
CHECK STD (~20 ppt)	0.009134	21.07
CHECK STD (~20 ppt)	0.009087	20.27

Finally, as it is known that UV radiation degrades organic material, UV treatment of the samples was undertaken. The samples in 5% BrCl were poured into pre-cleaned soda-lime glass vials, capped with teflon lined caps, and subjected to 24 hours of UV radiation. The samples were placed on a test-tube rack inside a black fiberglass box atop a motorized turntable. The box also contained a bank of UV lamps. The samples rotated on the turntable for 24 hours under UV light. Table E5 shows the results of this experiment. The UV treatment seems to have had no effect on the organic material and did not diminish the interference in the MA-2000. However, due to the fact that the gold trap was cleansed gradually after each absorbance decrease caused by a high-organic liquid sample, it seemed likely that something was interfering with the gold trap's ability to collect mercury. Five check standards containing no organics were required before the MA-2000 rebounded in its ability to analyze mercury.

Sample ID	Absorbance	Hg (ppt)
CRREL 15	0.000629	0.66
CHECK STD (~20 ppt)	0.000270	10.18
CHECK STD (~20 ppt)	0.000642	0.69
CHECK STD (~20 ppt)	0.002565	5.20
CHECK STD (~20 ppt)	0.007389	16.51
CHECK STD (~20 ppt)	0.00655	19.25
CRREL 19	0.000273	-0.18
CHECK STD (~20 ppt)	0.000246	-0.24
CHECK STD (~20 ppt)	0.000587	0.56
CHECK STD (~20 ppt)	0.002779	5.70
CHECK STD (~20 ppt)	0.007111	15.86
CHECK STD (~20 ppt)	0.008363	18.80

Because soda-lime glass is known to limit the transmission of UV radiation, we switched to quartz glass test tubes for UV treatment of samples. The experiment was repeated with quartz glass and was a resounding success. The quartz glass allowed for transmission of UV radiation and oxidation of the offending organics. After about 24 hours of UV treatment the interference within the MA-2000 had been eliminated (table E6).

Sample No.	Absorbance	Hg (ppt)	UV
05BW08HgU	0.000518	0.47	1.25 hrs
CHECK STD (~20 ppt)	0.000274	-0.11	
CHECK STD (~20 ppt)	0.001295	2.32	
CHECK STD (~20 ppt)	0.007176	16.31	
CHECK STD (~20 ppt)	0.008118	18.55	
CHECK STD (~20 ppt)	0.000356	0.08	
CHECK STD (~20 ppt)	0.003056	6.51	
CHECK STD (~20 ppt)	0.008128	18.57	
CHECK STD (~20 ppt)	0.004849	10.30	23 hrs
CHECK STD (~20 ppt)	0.008787	20.14	
CHECK STD (~20 ppt)	0.008832	20.25	

However, the quartz glass tubes used in this experiment were only a stop-gap measure. Their small diameter made sample transfer extraordinarily difficult and we could not effectively seal them. Because having custom quartz glass tubes made at the University of Michigan's glass shop would have been time consuming and expensive it was decided to order teflon vials (PFA) that would be easy to clean, easy transfer samples into and out of, and sealable with teflon stoppers. The vials were advertised as being able to transmit 100% of UV radiation, but this apparently turned out not to be the case. Whereas the interfering organics in the Alaskan water samples can be eliminated in quartz glass in approximately 24 hours, samples in the PFA vials require 3-5 days of UV treatment before the organics cease to interfere with the MA-2000's ability to trap and analyze mercury.

## References

- The Alaska Native Knowledge Network <[www.ankn.uaf.edu](http://www.ankn.uaf.edu)>.
- AMAP (2002). Arctic Pollution 2002 (Persistent Organic Pollutants, Heavy Metals, Radioactivity, Human Health, Changing Pathways). Oslo, Norway, Arctic Monitoring and Assessment Programme (AMAP).
- Ariya, P.A., Amyot, M., Schroeder, W.H., Raofie, F., Rhyjokov, A., Lalonde, J., and L. Barrie (2004). The Arctic: a sink for mercury, TELLUS, 2004.
- Barrow Area Information Database- Internet Map Server <[www.baidims.org](http://www.baidims.org)>.
- Benoit, J.M., Fitzgerald, W. F., and A. W. H. Damman (1998). The biogeochemistry of an ombrotrophic bog: evaluation of use as an archive of atmospheric mercury deposition. *Environmental Research, Sect. A* 78, 118-133.
- Biester, H., Kilian, R., Hertel, C., Woda, C., Mangini, A., and H.F. Sholer (2002). Elevated mercury concentrations in peat bogs of South Patagonia, Chile- an anthropogenic signal. *Earth and Planetary Science Letters*, 201, 609-620.
- Billings, W.D., and Peterson, K.M., 1980. Vegetational change and ice-wedge polygons through the thaw-lake cycle in arctic Alaska. *Arctic and Alpine Research*, 12:413-432.
- Bindler, R. (2003). Estimating the natural background atmospheric deposition rate of mercury utilizing ombrotrophic bogs in southern Sweden. *Environmental Science and Technology* 37(1): 40 -46.
- Booth, S. and D. Zeller (2005). Mercury, food webs, and marine mammals: implications of diet and climate change for human health. *Environmental Health Perspectives* 110(5): 521-526.
- Britton, M. E., 1966. Vegetation of the arctic tundra. In Hansen, H. P. (ed.) *Arctic Biology*. Oregon State University Press, Corvallis OR.
- Brown, J., Miller, P.L., Tieszen, L.L., and F. Bunnell. An Arctic ecosystem: the coastal tundra at Barrow, Alaska. Hutchinson & Ross, Stroudsburg, PA. 1980.
- Bullock, O.R. (2000) Modeling assessment of transport and deposition patterns of anthropogenic mercury air emissions in the United States and Canada. *The Science of the Total Environment* 259, 145-157.
- Douglas, T.A., Sturm, M., Simpson, W.R., Brooks, S., Lindberg, S.E., and D.K. Perovich (2005). Elevated mercury measured in snow and frost flowers near Arctic sea ice leads. *Geophysical Research Letters* 32.
- Drexel, R.T, Haitzer, M., Ryan, J.R., Aiken, G.R., and K.L. Nagy (2002). Mercury (II) sorption to two Florida Everglades peats: evidence for strong and weak binding and competition by dissolved organic matter released from the peat. *Environmental Science and Technology* 36, 4058-4064.
- Dvonch, J. T., Graney, J.R., Keeler, G.J., and R.K. Stevens (1999). Use of elemental tracers to source apportion mercury in south Florida precipitation. *Environmental Science and Technology* 31: 4522-4527.
- Ebinghaus, R., Kock, H.H., Temme, C., Einax, J.W., Löwe, A.G., Richter, A., Burrows, J.P., and W.H. Schroeder (2002). Antarctic springtime depletion of atmospheric mercury. *Environmental Science and Technology* 36(6): 1238-1244.
- Fitzgerald, W.F., Engstrom, D.R., Mason, R.P., and E.A. Nater (1998). The case for atmospheric mercury contamination in remote areas. *Environmental Science and Technology* 32(1): 1-7.

Fitzgerald, W.F., Lamborg, C.H., Tseng, C-M., Balcom, P.H. and C.R. Hammerschmidt (2005). Modern and historic atmospheric mercury fluxes in northern Alaska: global sources and arctic depletion. *Environmental Science and Technology* 39(2): 557 - 568.

FitzPatrick, E.A. (1997) Arctic soils and permafrost. In: Woodin, S.J. and Marquiss, M. (eds), *Ecology of Arctic Environments*. Special Publication Series of the British Ecological Society, Number 13. Blackwell Science, Ltd., Oxford, United Kingdom.

Givelet, N., Roos-Barracough, F., and W. Shotyk (2003). Predominant anthropogenic sources and rates of atmospheric mercury accumulation in southern Ontario recorded by peat cores from three bogs: comparison with natural "background" values (past 8000 years). *Journal of Environmental Monitoring* 5: 935-949.

Givelet, N., Roos-Barracough, F., Goodsite, M.E., Cheburkin, A., and W. Shotyk (2004a). Atmospheric mercury accumulation rates between 5900 and 800 calibrated years bp in the high Arctic of Canada recorded by peat hummocks. *Environmental Science and Technology* 38, 4964-4972.

Givelet, N., Le Roux, G., Cheburkin, A., Chen, B., Frank, J., Goodsite, M.E., Kempter, H., Krachler, M., Noernberg, T., Rausch, N., Rheinberger, S., Roos-Barracough, F., Sapkota, A., Scholz, C. and W. Shotyk (2004b). Suggested protocol for collecting, handling and preparing peat cores and peat samples for physical, chemical, mineralogical and isotopic analyses. *Journal of Environmental Monitoring* 6, 481-492.

Godish, Thad. *Air Quality* 4<sup>th</sup> Edition. Lewis Publishers. Boca Raton, FL. 2004.

Grandjean, P., Weihe, P., White, R.F., Debes, F., Araki, S., Yokoyama, K., Murata, K., Sorensen, N., Dahl, R., Jorgensen, P.J. (1997). Cognitive deficit in 7-year-old children with prenatal exposure to methylmercury. *Neurotoxicology and Teratology* 19 (6): 417-428.

Hammerschmidt, C.R., Fitzgerald, W.F., Lamborg, C.H., Balcom, P.H., and C-M Tseng (2006). Biogeochemical cycling of methylmercury in lakes and tundra watersheds of Arctic Alaska. *Environmental Science and Technology* 40: 1204-1211.

Hillel, D (1982). *Introduction to Soil Physics*. Academic Press, Inc. San Diego.

Hinkel, K.M., Eisner, W.R., Brockheim, J.G., Nelson, F.E., Peterson, K.M., and X. Dai (2003). Spatial extent, age, and carbon stocks in drained thaw lake basins on the Barrow Peninsula, Alaska. *Arctic, Antarctic, and Alpine Research* 35, 291-300.

Hogan, J.M. (2005) Hydrologic behaviour and hydraulic properties of a patterned fen in Saskatchewan. A thesis submitted to the college of graduate studies and research, University of Saskatchewan. <[library.usask.ca/theses/available/etd-01302006-151353](http://library.usask.ca/theses/available/etd-01302006-151353)>.

Hopkins, D.M., 1949. Thaw lakes and thaw sinks in the Imuruk Lake area, Seward Peninsula. *Journal of Geology*, 57: 119-131.

Hussey, K. M. and Michelson, R. W., 1966. Tundra relief features near Point Barrow, Alaska. *Arctic*, 19: 162-184.

Hylander, L.D. and M. Meili, 2003. 500 years of mercury production: global annual inventory by region until 2000 and associated emissions. *Science of the Total Environment* 304, 13-27.

Jensen A. and A. Jensen (1991). Historic rates of mercury in Scandinavia estimated by dating and measurement of mercury in cores of peat bogs. *Water, Air, and Soil Pollution* 56, 769-777.

Lamborg, C.H.F., Fitzgerald, W.F., Damman, A.W.H., Benoit, J.M., Balcom, P.H., and D.R. Engstrom (2002). Modern and historic atmospheric mercury fluxes in both hemispheres; global and regional mercury cycling implications. *Global Biogeochemical Cycles* 16(4): 1104.

- Lindberg, S.E., Brooks, S., Lin, C.J., Scott, K.J., Landis, M.S., Stevens, R.K., Goodsite, M.E., and A. Richter (2002). Dynamic oxidation of gaseous mercury in the Arctic troposphere at polar sunrise. *Environmental Science and Technology* 36, 1245-1256.
- Lindqvist, O., Johansson, K., Bringmark, L., Timm, B., Aastrup, M., Andersson, A., Hovsenius, G., Håkanson, L., Iverfeldt, A., and M. Meili (1991). Mercury in the Swedish environment- recent research on causes, consequences and corrective methods. *Water, Air, and Soil Pollution* 55: 23-30.
- Lodenius, M., Ari, S., and U-R Antti (1983). Sorption and mobilisation of mercury in peat soil. *Chemosphere* 12: 1575 -1581.
- Losetto, L.L., Lean, D.R.S., and S.D. Siciliano (2004). Snowmelt sources of methylmercury to high arctic ecosystems. *Environmental Science and Technology* 38: 3004-3010.
- Lu, J.Y., Schroeder, W.H., Barrie, L.A., Steffen, A., Welch, H.E., Martin, K., Lockhart, L., Hunt, R.V., Boila, G. and A. Richter (2001). Magnification of atmospheric mercury deposition to polar regions in the springtime; the link to troposphere ozone depletion chemistry. *Geophysical Research Letters* 28 (17), 3219-3222.
- Mackay, J.R., 1988. Catastrophic lake drainage, Tukoyaktuk Peninsula area, District of Mackenzie. *Current Research, Part D. Geological Survey of Canada. Paper 88-1D: 83-90.*
- Martinez-Cortizas, A.M., Pontevedra Pomba X., Garcia-Rodeja E., Novoa Munoz J.C., and W. Shotyk, 1999. Mercury in a Spanish peat bog: archive of climate change and atmospheric metal deposition. *Science* 284, 939-942.
- Mason, R.P.F., Fitzgerald, W.F. and F.M.M. Morel (1994). The biogeochemical cycling of elemental mercury: anthropogenic influences. *Geochimica et Cosmochimica Acta* 58(15): 3191-3198.
- Morel, F.M.M., Kraepiel, A.M.L., and M. Amyot (1998). The chemical cycle and bioaccumulation of mercury. *Annual Review of Ecological Systems* 29: 543-566.
- Myers, G.J., Davidson, P.W., Cox, C., Shamlaye, C.F., Palumbo, D., Cernichiari, E., Sloane-Reeves, J., Wilding, G.E., Kost, J., Huang, L-S., and T.W. Clarkson (2003). Prenatal methylmercury exposure from ocean fish consumption in the Seychelles child development study. *Lancet* 361: 1686-1692.
- National Atmospheric Deposition Program Mercury Deposition Network Mercury Deposition Summary Report, 2004). <http://nadp.sws.uiuc.edu/lib/data/2004as.pdf>.
- National Climate Data Center data. <[www.ncdc.noaa.gov](http://www.ncdc.noaa.gov)>.
- Nettleton, L. (2005). Visualizing Frost Boils. *Challenges in Science and Engineering* 13(1). Arctic Region Supercomputing Center. <[www.arsc.edu/challenges/2005/frostboils.html](http://www.arsc.edu/challenges/2005/frostboils.html)>.
- Norton S.A., Evans G.C., and J.S. Kahl (1997). Comparison of Hg and Pb fluxes to hummocks and hollows of ombrotrophic Big Heath Bog and to nearby Sargent Mt. Pond, Maine, USA. *Water, Air, and Soil Pollution* 100, 271-286.
- Nriagu, J. (1989). A Global Assessment of Natural Sources of Atmospheric Trace Metals. *Nature* 338: 47-49.
- Oechel, W.C., Cook, A.C., Hastings, S.J., and G.L. Vourlitis (1997). Effects of CO<sub>2</sub> and climate change on arctic ecosystems. In: Woodin, S.J. and Marquiss, M. (eds), *Ecology of Arctic Environments. Special Publication Series of the British Ecological Society, Number 13. Blackwell Science, Ltd., Oxford, United Kingdom.*
- Outridge, P.M., Hobson, K.A., McNeely, R. and A. Dyke (2002). A comparison of modern and preindustrial levels of mercury in the teeth of beluga in the Mackenzie Delta, Northwest Territories, and walrus at Igloolik, Nunavut, Canada. *Arctic* 55 (2): 123-132.

- Pheiffer-Madsen P., 1981. Peat bog records of atmospheric mercury deposition. *Nature* 293, 127-129.
- Poissant, L., Pilote, M., Xu, X. Zhang, H., and C. Beauvais (2004). Atmospheric mercury speciation and deposition in the Bay St. Francois wetlands. *Journal of Geophysical Research, D, Atmospheres* 109(11).
- Poulain, A.J., Lalonde, J.D., Amyot, M., Shead, J.A., Raofic, F., and P.A. Ariya (2004). Redox transformations of mercury in an Arctic snowpack at springtime. *Atmospheric Environment* 38: 6763–6774.
- Rember, R.D. and J.H. Trefry (2004). Increased concentrations of dissolved trace metals and organic carbon during snowmelt in rivers of the Alaskan Arctic. *Geochimica et Cosmochimica Acta* 68(3): 477– 489
- Rissanen, T., Voutilainen, S., Nyysönen, K., Lakka, T.A., and J.T. Salonen (2000). Fish oil-derived fatty acids, docosahexaenoic acid and docosapentaenoic acid, and the risk of acute coronary events: the kuopio ischaemic heart disease risk factor study. *Circulation* 102(22), 2677-2679.
- Roos-Barracough, F., Martinez-Cortizas, A., Garcia-Rodeja, E., and W. Shotyk. (2002a). A 14,500 year record of the accumulation of atmospheric mercury in peat: volcanic signals, anthropogenic influences and a correlation to bromine accumulation. *Earth and Planetary Science Letters* 202, 435-451.
- Roos-Barracough, F., Givélet, N., Martinez-Cortizas, A., Goodsite, M.E., Biester, H., and Shotyk W (2002b). An analytical protocol for the determination of total mercury concentrations in solid peat samples. *Science of the Total Environment* 292(1-2),129-139.
- Roos-Barracough, F. and W. Shotyk (2003). Millennial-scale records of atmospheric mercury deposition obtained from ombrotrophic and minerotrophic peatlands in the Swiss Jura Mountains. *Environmental Science and Technology* 37, 235-244.
- St. Louis, V.L., Sharp, M.J., Steffen, A., May, A., Barker, J., Kirk, J.L., Kelly, D.J.A., Arnott, S.E., Keatley, B., and J.P. Smol (2005). Some sources and sinks of monomethyl and inorganic mercury on Ellesmere Island in the Canadian high Arctic. *Environmental Science and Technology* 39: 2686-2701.
- Schuster, P.F., Krabbenhoft, D.P., Naftz, D.L., Cecil, L.D., Olson, M.L., Dewild, J.F., Susong, D.D., Green, J.R., and M. Abbott (2002). Atmospheric mercury deposition during the last 270 years: a glacial ice core record of natural and anthropogenic sources. *Environmental Science & Technology* 36(11), 2302-2310.
- Schroeder, W.H., Anlauf, K.G., Barrie, L.A., Lu, J.Y., Steffen, A., Scheeberger, D.R., and T. Berg (1998). Arctic springtime depletion of mercury. *Nature* 394, 331-332.
- Shanley, J.B., Schuster, P.F., Reddy, M.R., Roth, D.A., Taylor, H.E., and G.R. Aiken (2002). Mercury on the move during snowmelt in Vermont. *Eos* 83(5).
- Shotyk, W (1988). Review of the inorganic geochemistry of peats and peatland waters. *Earth Science Reviews* 25: 95-176.
- Shotyk, W., Goodsite, M.E., Roos-Barracough, F., Frei, R., Heinemeier, J., Asmund, G., Lohse, C., and T.S. Hansen (2003). Anthropogenic contributions to atmospheric Hg, Pb and As accumulation recorded by peat cores from southern Greenland and Denmark dated using the  $^{14}\text{C}$  “bomb pulse curve”. *Geochimica et Cosmochimica Acta* 67(21): 3991–4011.
- Shotyk, W., Goodsite, M.E., Roos-Barracough, F., Givélet, N., Le Roux, G., Weiss, D., Cheburkin, A.K., Knudsen, K., Heinemeier, J., van der Knaap, W.O., Norton, S.A., and C. Lohse (2005). Accumulation rates and predominant atmospheric sources of natural and anthropogenic Hg and Pb on the Faroe Islands. *Geochimica et Cosmochimica Acta* 69(1): 1-17.
- Shur, Y., Ping, C-L and M. T. Jorgenson (2006). Soil Formation in Frost-boil Environments. Abstracts of the 18<sup>th</sup> World Congress on Soil Science. <[crops.confex.com/crops/wc2006/techprogram/P18440.HTM](http://crops.confex.com/crops/wc2006/techprogram/P18440.HTM)>

Skov, H., Christensen, J.H., Goodsite, M.E., Heidam, N.Z., Jensen, B., Wahlin, P., and G. Geernaert (2004). Fate of elemental mercury in the Arctic during atmospheric depletion episodes and the load of atmospheric mercury to the Arctic. *Environmental Science and Technology* 38, 2373-2382.

Steinnes, E. and T.E. Sjobakk (2005). Order-of-magnitude increase of Hg in Norwegian peat profiles since the outset of industrial activity in Europe. *Environmental Pollution* 137(2): 365-370.

Weihe, P., Grandjean, P., Debes, F., and R. White (1996). Health implications for Faroe islanders of heavy metals and PCBs from pilot whales. *Science of the Total Environment* 186(1-2):141-148.

Zahir, F., Rizwi, S.J., Haq, S.K., and R.H. Khan (2005). Low dose mercury toxicity and human health. *Environmental Toxicology and Pharmacology* 20: 351-360.